Inorganic Chemistry

Article

pubs.acs.org/IC

Metal and Ligand Effects on Bonding in Group 6 Complexes of Redox-Active Amidodiphenoxides

Leila G. Ranis,[†] Kalpani Werellapatha,[‡] Nicholas J. Pietrini,[†] Bruce A. Bunker,[‡] and Seth N. Brown*,[†]

[†]Department of Chemistry and Biochemistry and [‡]Department of Physics, University of Notre Dame, 251 Nieuwland Science Hall, Notre Dame, Indiana 46556-5670, United States

Supporting Information

ABSTRACT: Group 6 complexes $M(ONO)_2$ (M = Cr, Mo, W; ONO = bis(2-oxy-3,5-di-*tert*-butylphenyl)amide) are prepared by the reaction of divalent metal halide precursors with $Pb(ONO^{Q})_2$. Analogous complexes containing the 2,4,6,8-tetra-*tert*-butyl-1,9-dioxophenoxazinate ligand (DOPO) are prepared by protonolysis of chromocene with $H(DOPO^{Q})$ or by reaction of $Pb(DOPO^{Q})_2$ with $M_2Br_4(CO)_8$ (M = Mo, W). The molybdenum and tungsten complexes are symmetrical, octahedral compounds for which spectroscopic data are consistent with M(VI) complexes with fully reduced $[L^{Cat}]^{3-}$ ligands. Quantitative analysis of the intraligand bond lengths, by comparison with literature standards, allows calculation of metrical oxidation states (MOS) for the ONO ligands. The MOS values of the tungsten and molybdenum complexes indicate that π donation from the ligand is weak and that differences between the ONO and DOPO ligands are small. In both the solid state and in solution, $Cr(DOPO)_2$ is paramagnetic with localized quinone and semiquinone ligands bound to Cr(III). The geometry and electronic structure of $Cr(ONO)_2$ differ in the solid state and in solution, as determined by crystallography, magnetic measurements, and Cr K-edge X-ray absorption spectroscopy. In solution, the structure resembles that of the DOPO analogue. In contrast, solid $Cr(ONO)_2$ is a singlet, and X-ray absorption near-edge spectroscopy indicates that the chromium is significantly more oxidized in the solid state than in solution. An electronic description compounds to that of the tungsten and molybdenum analogues, but with considerably more charge transfer from the ligand to chromium via π donation, is in agreement with the experimental observations.

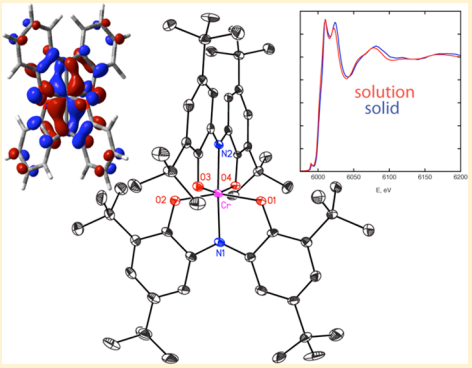

INTRODUCTION

Redox-active ligands continue to fascinate and perplex chemists, since their ability to adopt multiple stable oxidation states often makes the electronic structures of their metal complexes difficult to analyze.[1] The resultant ambiguities in metal oxidation states have earned this class of ligands the moniker "noninnocent." An exemplary and widely studied member of this class is the 3,5-di-*tert*-butyl-1,2-quinone-1-(2-oxy-3,5-di-*tert*-butylphenyl)imine or ONO ligand (Figure 1). While the ONO ligand was first introduced in group 14 $(ONO^{SQ})MX_2$ complexes,[2] it has subsequently been used extensively as a ligand for transition metals, including several that are catalytically active in oxidation reactions.[3] Bis-ligand $M(ONO)_2$ complexes are especially widely distributed, not only among first-row transition metals but also in the s- and p-blocks (Figure 2). These complexes have been examined extensively in terms of their structural[4] and magnetic[5,6] properties.

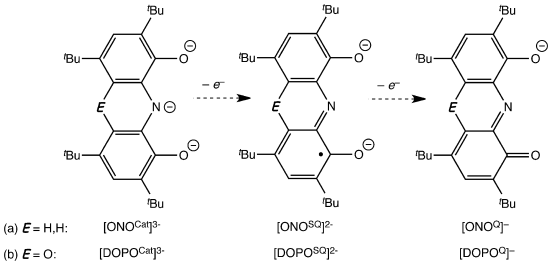

Figure 1. Oxidation states of (a) ONO and (b) DOPO ligands.

	Mg[7]												Al[8]	Si[9,10]		
	Ca[8]		Ti[5]	V[5]	Cr	Mn[11]	Fe[7,4]	Co[11]	Ni[7,4]	Cu[7,12]	Zn[7,13]	Ga[8]	Ge[5]			
	Sr[14]				Mo		Ru[15]				Cd[7]		Sn[16,17]			
	Ba[8,14]				W[18]		Os[15]						Pb[16,10]			

Figure 2. Periodic table of the $M(ONO)_2$ complexes. Entries in boldface have been characterized structurally. Entries in red are from this work.

Received: May 25, 2014
Published: September 23, 2014

   dx.doi.org/10.1021/ic501222n | *Inorg. Chem.* 2014, 53, 10203−10216

In particular, the 3d elements form a nearly complete set of $M(ONO)_2$ compounds, with only chromium and scandium missing from the series (though the homoleptic tris complex $Sc(ONO)_3$ has been prepared[19]). The gap at group 6 is unfortunate, since the middle of the periodic table is where the most interesting questions of electronic structure arise. Early transition metals (such as Ti,[5] V,[20] and W[18]) adopt a d^0 configuration; later transition metals (Ni, Cu, and Zn) adopt divalent oxidation states since their higher oxidation states are not readily accessible. Here we report the preparation and characterization of both $Cr(ONO)_2$ and $Mo(ONO)_2$, which completes the set of group 6 complexes and allows for a systematic comparison of structure and bonding down a group. We also prepared the three homoleptic group 6 complexes of a modified ONO ligand in which the two rings are joined by an oxygen bridge (Figure 1b). This dioxophenoxazine, or DOPO, ligand was recently prepared,[21] and its properties were examined in a number of first-row transition metal $(DOPO)_2M$ complexes.[22] The group 6 complexes of this ligand provide additional insights into the effects of ligand geometric and electronic properties on the electronic structures of complexes with redox-active ligands.

EXPERIMENTAL SECTION

Unless otherwise noted, all procedures were carried out under an inert atmosphere in a nitrogen-filled glovebox or on a vacuum line. Chlorinated solvents and acetonitrile were dried over 4 Å molecular sieves, followed by CaH_2. Benzene and toluene were dried over sodium, and ether and tetrahydrofuran (THF) were dried over sodium benzophenone ketyl. Deuterated solvents were obtained from Cambridge Isotope Laboratories, dried using the same procedures as their protio analogues, and stored in the drybox prior to use. $Pb(ONO^Q)_2$ was prepared by a modification[10] of the method of McGarvey and co-workers.[16] 2,6-Dihydroxy-3,5-di-*tert*-butylaniline was prepared using the method of Minkin and co-workers.[21] $Mo_2Br_4(CO)_8$[23] and $W_2Br_4(CO)_8$[24] were prepared using literature procedures. All other reagents were commercially available and used without further purification. Routine NMR spectra were measured on $CDCl_3$ solutions on a Varian VXR-300 or Bruker DPX-400 spectrometer. Chemical shifts for ^1H and $^{13}C\{^1H\}$ spectra are reported in ppm downfield of tetramethylsilane, with spectra referenced using the known chemical shifts of the solvent residuals. UV−visible−near-infrared (UV−vis−NIR) spectra were obtained as solutions in CH_2Cl_2 on Beckman DU-7500, Thermo Scientific Evolution Array, or Jasco V-670 spectophotometers. Infrared spectra were recorded as solids using an attenuated total reflection attachment and a Jasco FT/IR-6300 spectrometer. Elemental analyses were performed by M−H−W Laboratories (Phoenix, AZ) or Robertson Microlit Laboratories (Ledgewood, NJ).

Bis[bis(3,5-di-*tert*-butyl-2-oxyphenyl)amido]chromium, Cr(ONO)$_2$. Under a nitrogen atmosphere, 16.9 mg of anhydrous $CrCl_2$ (Alfa Aesar, 0.138 mmol) was dissolved in 20 mL of THF. To this solution was added a solution of $Pb(ONO^Q)_2$ (146.0 mg, 0.139 mmol) in THF, and the mixture was stirred for 5 h under N_2. The mixture was then gravity filtered in the air to remove precipitated $PbCl_2$, the solvent was removed on a rotary evaporator, and the residue was dissolved in dichloromethane. The CH_2Cl_2 solution was chromatographed on silica gel, eluting with dichloromethane, and the fast-moving brown band (moving ahead of a slower-moving blue band) was collected. The solvent was evaporated from the eluate, and the solid residue was slurried in 5 mL of ether, collected by suction filtration, washed with 5 mL of ether, and air-dried for 15 min to furnish 64.6 mg of $Cr(ONO)_2$ as a black crystalline solid (52%). ^1H NMR: δ 1.16, 1.25 (sl br s, 36H ea., ^{t}Bu), 37.55, 47.96 (br s, 4H ea., Ar*H*). IR (cm^{-1}): 2955 (s), 2906 (m), 2867 (m), 1580 (m), 1459 (m), 1418 (w), 1360 (s), 1307 (m), 1280 (s), 1240 (vs), 1195 (s), 1165 (s), 1107 (m), 1091 (m), 1048 (s), 1022 (s), 1009 (s), 933 (w), 902 (s), 850 (s), 829 (w), 818 (w), 776 (m), 732 (s), 669 (w). UV−vis: λ_{max} = 349 nm (ε = 14 400 M^{-1} cm^{-1}), 450 (10 500), 510 (sh, 7500), 633 (sh, 5500), 670 (sh, 6500), 770 (7300), 850 (sh, 6600), 1025 (sh, 3200). Electrospray ionization mass spectrometry (ESI-MS): 897.5620 ($M+H^+$, calcd 897.5601; isotope pattern shows a mixture of M^+ and $M+H^+$). Anal. Calcd for $C_{56}H_{80}CrN_2O_4$: C, 74.96; H, 8.99; N, 3.12. Found: C, 74.86; H, 8.84; N, 3.10%.

Bis[bis(3,5-di-*tert*-butyl-2-oxyphenyl)amido]molybdenum, Mo(ONO)$_2$. In a 20 mL vial in the drybox, 97.6 mg of $Mo_2Br_4(CO)_8$ (0.265 mmol Mo) and 279.6 mg of $Pb(ONO^Q)_2$ (0.266 mmol, 1.00 equiv) were combined. Dichloromethane (10 mL) was added, and the mixture was swirled gently for 3 min as CO evolved. A stirbar was then added to the vial, the vial was capped and removed from the drybox, and the dark red reaction mixture was stirred under N_2 for 1 h. After allowing the mixture to stand for a further 3 h without stirring, the vial was opened to the air, and the solution was gravity filtered to remove $PbBr_2$. The CH_2Cl_2 was removed using a rotary evaporator, and the solid residue was slurried in 5 mL of acetonitrile, collected by suction filtration, washed with 2 × 5 mL CH_3CN, and air-dried for 30 min to give 134.4 mg of $Mo(ONO)_2$ as a black crystalline solid (54%). The analytical sample was filtered through a short plug of silica gel, eluting with CH_2Cl_2, to remove traces of $PbBr_2$. ^1H NMR ($CDCl_3$): δ 1.29, 1.34 (s, 36H ea., ^{t}Bu), 6.75, 7.02 (d, 2 Hz, 4H ea., Ar*H*). $^{13}C\{^1H\}$ NMR ($CDCl_3$): δ 29.77, 31.80 ($C(CH_3)_3$), 34.90, 35.10 ($C(CH_3)_3$), 111.74, 122.44, 136.51, 137.76, 145.58, 167.50 (*O*C). IR (cm^{-1}): 2954 (s), 1592 (m), 1474 (m), 1453 (m), 1402 (m), 1361 (s), 1294 (w), 1244 (s), 1158 (m), 1050 (m), 1011 (m), 934 (w), 908 (m), 849 (m), 834 (m), 762 (m), 732 (s), 697 (s), 676 (s). UV−vis (CH_2Cl_2): λ_{max} = 297 nm (ε = 23 700 M^{-1} cm^{-1}), 505 (26 300), 800 (sh, 780). Anal. Calcd for $C_{56}H_{80}MoN_2O_4$: C, 71.46; H, 8.57; N, 2.98. Found: C, 71.45; H, 8.30; N, 3.21%.

Bis[bis(3,5-di-*tert*-butyl-2-oxyphenyl)amido]tungsten, W(ONO)$_2$. A mixture of $W_2Br_4(CO)_8$ (512.7 mg, 1.125 mmol W) and $Pb(ONO^Q)_2$ (1.1967 g, 1.137 mmol, 1.01 equiv) was dissolved in 10 mL of dry CH_2Cl_2 in a 20 mL vial and stirred uncovered for 5 min in the drybox until vigorous gas evolution abated. More CH_2Cl_2 (5 mL) was added, the vial was capped, and the solution was allowed to stir for 40 min under N_2. The solution was opened to the air, diluted to 50 mL with CH_2Cl_2, and gravity filtered to remove $PbBr_2$. The filtrate was evaporated to dryness on the rotary evaporator, and the residue was slurried in 15 mL of CH_3CN. The solid was isolated by suction filtration on a glass frit, washed thoroughly with 2 × 5 mL of CH_3CN, and air-dried for 20 min to yield 0.4795 g (41%) of dark brown $W(ONO)_2$. ^1H NMR ($CDCl_3$): δ 1.24, 1.38 (s, 36H ea., ^{t}Bu), 6.72, 7.25 (d, 2 Hz, 4H ea., Ar*H*). $^{13}C\{^1H\}$ NMR ($CDCl_3$): δ 29.73, 32.00 ($C(CH_3)_3$), 34.87, 35.02 ($C(CH_3)_3$), 112.47, 120.65, 136.17, 138.62, 145.47, 161.91 (*O*C). IR (cm^{-1}): 2954 (m), 1598 (w), 1568 (w), 1476 (m), 1413 (s), 1361 (m), 1325 (w), 1290 (w), 1240 (s), 1208 (m), 1135 (w), 1050 (m), 1012 (m), 936 (m), 910 (m), 872 (m), 838 (s), 741 (s), 677 (s). Anal. Calcd for $C_{56}H_{80}N_2O_4W$: C, 65.36; H, 7.84; N, 2.72. Found: C, 65.35; H, 7.62; N, 2.67%.

2,4,6,8-tetra-*tert*-butyl-9-hydroxy-1*H*-phenoxazin-1-one, H(DOPO^Q). This material was synthesized by a modification of the published procedure.[21] In a 250 mL Erlenmeyer flask, in the air, 761.7 mg of 3,5-di-*tert*-butylcatechol (Aldrich, 3.43 mmol) and 813.1 mg of 2,6-dihydroxy-3,5-di-*tert*-butylaniline (1 equiv) were dissolved in 25 mL of benzene. A catalytic amount of triethylamine (Aldrich, 107 μL, 10 mol %) was added, and the flask was sealed with Parafilm. After stirring for 24 h, the solvent was evaporated in vacuo at room temperature to give a purple oil that hardened into a glass. The solid was triturated with methanol and suction filtered over a fine porosity glass frit to recover purple crystalline $H(DOPO^Q)$, 380.8 mg (25%). Material prepared in this way is often contaminated with traces (<5%) of 2,4,6,8-tetra-*tert*-butylphenoxazin-1-one.[25] This impurity can be removed by chromatography,[21] but the compound was used without further purification in the following syntheses. ^1H NMR ($CDCl_3$): δ 1.38, 1.48 (s, 18H each, ^{t}Bu), 7.49 (s, 2H, Ar*H*) (ref 21 δ 1.39, 1.44, 7.45). $^{13}C\{^1H\}$ NMR ($CDCl_3$): δ 29.36, 30.29 ($C(CH_3)_3$), 34.33, 35.09 ($C(CH_3)_3$), 123.41, 133.61 (br), 134.77, 135.23, 141.00, 166.35 (br, *C*O).

dx.doi.org/10.1021/ic501222n | Inorg. Chem. 2014, 53, 10203−10216

Bis(2,4,6,8-tetra-*tert*-butyl-1,9-dioxophenoxazinato)lead(II), Pb(DOPO^{Q})$_2$. Method A. In a 250 mL round-bottom flask, in the air, 122.1 mg of lead acetate trihydrate (Aldrich, 0.322 mmol) and 280.2 mg of H(DOPO^{Q}) (1.99 equiv) were dissolved in 120 mL of methanol. The flask was sealed with a rubber septum, vented by a needle, and stirred in a 70 °C oil bath for 48 h. After it stood at room temperature overnight, the reaction mixture was suction filtered through a glass frit, and the matte blue precipitate was washed with 10 mL of methanol. The precipitate was dissolved in 10 mL of chloroform, and the solution was gravity filtered through filter paper to remove unreacted lead acetate. The filtrate was evaporated on a rotary evaporator, and the solid was slurried in acetonitrile, then suction filtered to give 153.4 mg of Pb(DOPO^{Q})$_2$ (44%). **Method B.** Lead(II) 2-ethylhexanoate (Strem, 0.551 g, 1.12 mmol) was weighed into a 20 mL scintillation vial and dissolved in 3 mL of CH_2Cl_2. To this solution was added a dark purple solution of H(DOPO^{Q}) (0.995 g, 2.27 mmol, 2.03 equiv) in 4 mL of CH_2Cl_2, causing an immediate color change to dark blue. To the solution was added 5 mL of acetonitrile, causing precipitation of a fine blue solid. After it stood for 1 h, the pasty mixture was suction filtered on a glass frit, and the precipitate was washed thoroughly with 10 mL of acetonitrile followed by 10 mL of CH_3OH and then air-dried for 2 h. A second crop was isolated after allowing the mixture of the filtrate and the acetonitrile wash to evaporate to half its original volume, giving a combined yield of 0.965 g Pb(DOPO^{Q})$_2$ (80%). ^{1}H NMR ($CDCl_3$): δ 1.19, 1.44 (s, 36H each, ^{t}Bu), 7.46 (s, 4H, Ar*H*). ^{13}C{^{1}H} NMR ($CDCl_3$): δ 29.10, 30.33 (C(*C*H$_3$)$_3$), 33.95, 34.98 (*C*(CH$_3$)$_3$), 119.40 (aromatic *C*H), 133.86, 136.22, 137.60, 143.41, 173.78 (*C*O). IR (cm^{-1}): 2954 (w), 2910 (w), 2867 (w), 1614 (w), 1589 (w), 1577 (m), 1510 (m), 1491 (m), 1453 (m), 1393 (m), 1384 (w), 1360 (m), 1350 (s), 1335 (m), 1325 (m), 1279 (m), 1245 (m), 1229 (m), 1205 (m), 1193 (m), 1166 (m), 1082 (m), 1071 (m), 1033 (m), 1021 (w), 998 (s), 982 (m), 928 (w), 908 (w), 898 (w), 876 (m), 806 (w), 791 (w), 779 (w), 774 (w), 740 (m), 731 (w), 698 (m), 659 (w), 614 (m), 602 (w), 596 (w), 545 (w), 530 (w), 516 (w), 510 (m). UV–vis (CH_2Cl_2): λ_{max} = 254 nm (sh, ε = 31 700 M^{-1} cm^{-1}), 299 (sh, 21 500), 402 (sh, 21 100), 708 (16 400). ESI-MS: 1081.5530 (M$^+$ + H, calcd 1081.5548). Anal. Calcd for $C_{56}H_{76}N_2O_6Pb$: C, 62.25; H, 7.09; N, 2.59. Found: C, 62.05; H, 7.00; N, 2.59%.

Bis(2,4,6,8-tetra-*tert*-butyl-1,9-dioxophenoxazinato)-chromium, Cr(DOPO)$_2$. In the drybox, 54.4 mg of chromocene (Strem, 0.299 mmol) and 251.2 mg of H(DOPO^{Q}) (1.92 equiv) were weighed into a 20 mL scintillation vial and dissolved in 4 mL of toluene. The vial was capped and allowed to stand overnight at room temperature. The sample was taken out of the drybox, and the solvent was removed on the rotary evaporator. The solid residue was slurried in 20 mL of acetonitrile before suction filtration through a fine porosity glass frit to yield crude Cr(DOPO)$_2$ (220 mg). The crude product was dissolved in the air in 4 mL of benzene and layered with 8 mL of acetonitrile. Crystals were harvested after 24 h and washed with 10 mL of CH_3CN to give 160.5 mg of Cr(DOPO)$_2$ (60%). ^{1}H NMR ($CDCl_3$): δ 1.38 (br, 36H, ^{t}Bu), 2.60 (br s, 36H, ^{t}Bu), 49.27 (v br s, 4H, Ar*H*). IR (cm^{-1}): 2956 (w), 2910 (w), 2869 (w), 1608 (w), 1584 (w), 1538 (w), 1528 (w), 1498 (m), 1481 (w), 1468 (w), 1428 (w), 1405 (m), 1387 (w), 1359 (w), 1350 (w), 1333 (w), 1309 (m), 1285 (m), 1248 (m), 1194 (w), 1158 (w), 1089 (m), 1068 (w), 1052 (w), 1042 (m), 1024 (w), 1010 (m), 927 (w), 908 (w), 876 (m), 826 (w), 794 (w), 777 (w), 761 (w), 745 (w), 716 (w), 695 (m), 668 (w), 657 (w), 646 (w), 640 (w), 618 (w), 609 (w), 598 (w), 586 (w), 581 (w), 576 (w), 568 (w), 561 (w), 556 (w), 552 (w), 545 (w), 539 (w), 525 (m), 519 (m), 511 (m), 505 (s). UV–vis (CH_2Cl_2): λ_{max} = 255 nm (sh, ε = 32 800 M^{-1} cm^{-1}), 279 (sh, 26 200), 362 (17 400), 416 (23 100), 539 (sh, 4000), 688 (8100), 765 (sh, 6000). ESI-MS: 924.4927 (M$^+$, calcd 924.5109). Anal. Calcd for $C_{56}H_{76}N_2O_6Cr$: C, 72.70; H, 8.28; N, 3.03. Found: C, 71.63; H, 8.60; N, 2.91%.

Bis(2,4,6,8-tetra-*tert*-butyl-1,9-dioxophenoxazinato)-tungsten(VI), W(DOPO^{Cat})$_2$. In the drybox, 64.1 mg of $W_2Br_4(CO)_8$ (0.070 mmol) and 153.4 mg of Pb(DOPO^{Q})$_2$ (0.142 mmol, 1.01 mol per mol W) were weighed into a 20 mL scintillation vial and dissolved in 4 mL of chloroform. Immediately, carbon monoxide evolution was observed. The vial was capped, and the reaction mixture was stirred overnight at room temperature. The reaction mixture was then gravity filtered in the air, and the filtrate was evaporated to dryness on the rotary evaporator. The brown residue was triturated with acetonitrile and suction filtered on a fine porosity glass frit to recover W(DOPO^{Cat})$_2$ as an amber brown solid (123.9 mg, 72%). The analytical sample was filtered through a short plug of silica gel, eluting with CH_2Cl_2. ^{1}H NMR ($CDCl_3$): δ 1.28, 1.48 (s, 36H each, ^{t}Bu), 6.47 (s, 4H, Ar*H*). ^{13}C{^{1}H} NMR ($CDCl_3$): δ 29.44, 30.56 (C(*C*H$_3$)$_3$), 34.64, 34.68 (*C*(CH$_3$)$_3$), 125.47 (aromatic *C*H), 126.62, 128.46, 131.27, 141.94, 164.26 (*C*O). IR (cm^{-1}): 2953 (m), 2917 (w), 2869 (w), 1591 (w), 1499 (w), 1477 (w), 1457 (m), 1392 (w), 1362 (w), 1331 (w), 1305 (w), 1256 (w), 1234 (m), 1217 (m), 1175 (w), 1071 (s), 1031 (m), 1019 (m), 906 (w), 869 (w), 825 (w), 768 (m), 758 (m), 723 (w), 704 (m), 654 (m), 622 (w), 608 (w), 580 (m), 547 (s), 540 (s), 527 (m), 507 (s). UV–vis (CH_2Cl_2): λ_{max} = 412 nm (43 500 M^{-1} cm^{-1}), 469 (sh, 16 100). Anal. Calcd for $C_{56}H_{76}N_2O_6W$: C, 63.63; H, 7.25; N, 2.65. Found: C, 63.35; H, 7.44; N, 2.59%.

Bis(2,4,6,8-tetra-*tert*-butyl-1,9-dioxophenoxazinato)-molybdenum(VI), Mo(DOPO^{Cat})$_2$. Using the same procedure as for the tungsten analogue, 70.7 mg of $Mo_2Br_4(CO)_8$ (0.096 mmol) and 203.8 mg of Pb(DOPO^{Q})$_2$ (0.189 mmol, 0.98 equiv) were reacted in chloroform. The reaction mixture was allowed to stand for 2 h at room temperature before workup. Mo(DOPO^{Cat})$_2$ was isolated as a deep brown solid, 111.3 mg (61%). ^{1}H NMR ($CDCl_3$): δ 1.33, 1.45 (s, 36H each, ^{t}Bu), 6.62 (s, 4H, Ar*H*). ^{13}C{^{1}H} NMR ($CDCl_3$): δ 29.58, 30.60 (C(*C*H$_3$)$_3$), 34.56, 34.82 (*C*(CH$_3$)$_3$), 127.12 (aromatic *C*H), 127.80, 128.13, 132.25, 140.15, 168.29 (*C*O). IR (cm^{-1}): 2953 (m), 2918 (w), 2868 (w), 1744 (w), 1621 (w), 1578 (w), 1546 (w), 1497 (w), 1479 (w), 1449 (w), 1392 (w), 1362 (w), 1331 (w), 1302 (w), 1255 (w), 1238 (m), 1217 (m), 1176 (w), 1071 (s), 1037 (m), 1018 (w), 929 (w), 906 (w), 875 (m), 829 (w), 789 (w), 768 (m), 749 (w), 716 (w), 701 (m), 641 (m), 625 (m), 607 (w), 577 (m), 540 (s), 505 (s). UV–vis (CH_2Cl_2): λ_{max} = 312 nm (ε = 12 000 M^{-1} cm^{-1}), 463 (62 800), 605 (6500). ESI-MS: 971.4806 (M$^+$ + H, calcd 971.4758). Anal. Calcd for $C_{56}H_{76}N_2O_6Mo$: C, 69.40; H, 7.90; N, 2.89. Found: C, 69.68; H, 7.99; N, 2.85%.

Magnetic Susceptibility Measurements. To determine solid-state magnetic susceptibility, a weighed sample of the compound was placed on a weighed 2 cm × 2 cm square of parafilm. The parafilm was folded several times over to form a small pellet, taking care to prevent air bubbles. The pellet was put into one-half of a gel capsule. The other half of the capsule was packed tightly coaxially on top of the sample. The capsule was inserted into a straw and fixed in place an inch from the end by poking holes above and below where the capsule should sit. The magnetic susceptibility (χ_{meas}) of the sample at varying temperatures was measured using a Quantum Design Magnetic Property Measurement System (MPMS). The diamagnetic contribution to the susceptibility was estimated by multiplying the molar mass of the compound by 4.5 × 10^{-7} cm^3 mol^{-1} and was subtracted from the observed susceptibility.[26] Contributions from the sample holder were determined by measuring the magnetic susceptibility of the parafilm and gel capsule together and subtracting it from χ_{meas}.

Solution magnetic susceptibilities were determined using the Evans method.[27] Samples were dissolved in toluene-d_8 containing a known concentration of an inert standard (1,4-bis(trimethylsilyl)benzene or dimethyl terephthalate). The analyte solution was transferred into a screw-cap NMR tube, while a solution containing only the standard was pipetted into a coaxial insert. Shifts in the positions of the standard peaks in the presence and absence of analyte were measured at variable temperatures on a Varian VXR-500 spectrometer. Analyte concentration was corrected for the thermal expansion of the solvent[28] using literature data.[29]

Electrochemistry. Electrochemical measurements were performed in the drybox using a BAS Epsilon or Metrohm Autolab PGSTAT128N potentiostat. A standard three-electrode setup was used, with glassy carbon working and counter electrodes and a silver/silver chloride pseudoreference electrode. The electrodes were connected to the potentiostat through electrical conduits in the drybox wall. Samples were approximately 1 mM in CH_2Cl_2 with 100

dx.doi.org/10.1021/ic501222n | Inorg. Chem. 2014, 53, 10203–10216

Table 1. Crystal Data for $Cr(ONO)_2$, $Mo(ONO)_2$, $Pb(DOPO)_2{\cdot}2C_6H_6$, $Cr(DOPO)_2$, $Mo(DOPO)_2$, and $W(DOPO)_2$

	$Cr(ONO)_2$	$Mo(ONO)_2$	$Pb(DOPO)_2{\cdot}2C_6H_6$	$Cr(DOPO)_2$	$Mo(DOPO)_2$	$W(DOPO)_2$
empirical formula	$C_{56}H_{80}CrN_2O_4$	$C_{56}H_{80}MoN_2O_4$	$C_{68}H_{88}N_2O_6Pb$	$C_{56}H_{76}CrN_2O_6$	$C_{56}H_{76}MoN_2O_6$	$C_{56}H_{76}N_2O_6W$
formula weight	897.22	941.16	1236.59	925.19	969.13	1057.04
T (K)	100(2)	100(2)	120(2)	120(2)	120(2)	120(2)
λ (Å) (Mo Kα)	0.710 73	0.710 73	0.710 73	0.710 73	0.710 73	0.710 73
crystal system	triclinic	triclinic	orthorhombic	monoclinic	monoclinic	monoclinic
space group	$P\bar{1}$	$P\bar{1}$	*Pbca*	*C*2/*c*	$P2_1/c$	$P2_1/c$
refls. collected	21 334	25 290	205 665	78 768	38 852	71 487
indep. refls.	12 428	7584	15 345	10 974	10 868	13 261
R_{int}	0.0582	0.0740	0.0578	0.0496	0.1257	0.0354
obsd. refls. [$I > 2\sigma(I)$]	8668	5446	12 272	8408	6426	11 318
a (Å)	11.4672(7)	11.5456(12)	18.2299(17)	40.261(4)	20.518(2)	20.5540(12)
b (Å)	12.1310(5)	12.0570(13)	16.8979(16)	12.7201(11)	19.860(2)	19.8902(12)
c (Å)	20.6054(9)	20.4771(20)	39.677(4)	25.355(3)	12.9284(14)	12.9611(8)
α (deg)	83.393(3)	82.951(6)	90	90	90	90
β (deg)	73.886(5)	74.123(5)	90	124.543(4)	90.849(2)	91.0736(12)
γ (deg)	76.116(4)	76.035(6)	90	90	90	90
V (Å^3)	2669.7(2)	2655.8(5)	12222(2)	10695.7(19)	5267.5(10)	5297.9(6)
Z	2	2	8	8	4	4
crystal size, mm	0.17 × 0.12 × 0.02	0.27 × 0.08 × 0.03	0.24 × 0.19 × 0.06	0.25 × 0.19 × 0.13	0.23 × 0.12 × 0.04	0.19 × 0.14 × 0.12
number of refined params.	862	578	694	854	586	890
R indices [$I > 2\sigma(I)$][a]	$R1$ = 0.0611, $wR2$ = 0.1322	$R1$ = 0.0508, $wR2$ = 0.1099	$R1$ = 0.0371, $wR2$ = 0.0834	$R1$ = 0.0445, $wR2$ = 0.1096	$R1$ = 0.0503, $wR2$ = 0.0843	$R1$ = 0.0226, $wR2$ = 0.0514
R indices (all data)[a]	$R1$ = 0.0965, $wR2$ = 0.1588	$R1$ = 0.0873, $wR2$ = 0.1250	$R1$ = 0.0544, $wR2$ = 0.0897	$R1$ = 0.0657, $wR2$ = 0.1222	$R1$ = 0.1152, $wR2$ = 0.0970	$R1$ = 0.0315, $wR2$ = 0.0556
goodness-of-fit	1.028	1.040	1.083	1.023	0.912	1.043

[a] $R1 = \Sigma\,||F_o| - |F_c||/\Sigma|F_o|$; $wR2 = (\Sigma[w(F_o^2 - F_c^2)^2]/\Sigma w(F_o^2)^2)^{1/2}$.

mM Bu_4NPF_6 as the electrolyte. Potentials were referenced to ferrocene/ferrocenium at 0 V,[30] with the reference potential established by spiking the test solution with a small amount of ferrocene. Cyclic voltammograms were recorded with a scan rate of 120 mV/s.

Calculations. Geometry optimizations and orbital calculations used the hybrid B3LYP method, with an SDD basis set for the metal atom and a 6-31G* basis set for all other atoms, using the Gaussian09 suite of programs.[31] Starting geometries were generated from known crystal structures, with all *tert*-butyl groups replaced by hydrogen atoms, except that structures of $Cr(ONO)_2$ were also calculated with methyl groups and *tert*-butyl groups in the 3,5,3′,5′-positions. Optimized geometries were confirmed to be minima by frequency analysis. Plots of calculated Kohn−Sham orbitals were generated using the program GaussView (v. 5.0.8) with an isovalue of 0.04.

X-ray Absorption Spectroscopy. CrO_2 (Magtrieve, Aldrich) was used as a standard for chromium(IV), while sodium bis(dipicolinate)-chromium(III) dihydrate,[32] $Na[Cr(dipic)_2]{\cdot}2H_2O$, was used as a standard for chromium(III). The solid samples were prepared by spreading finely ground powders on Kapton tape and folding several times to achieve the desired thickness. Solution samples (10 mM in THF) were contained in nylon cells with Kapton windows attached with epoxy. The solid samples were fluorescence X-ray mapped above the Cr K-edge energy to find the most homogeneous spots in the sample.

Fluorescence chromium extended X-ray absorption fine structure (EXAFS) measurements were made at the Sector 10 Materials Research Collaborative Access Team (MRCAT), Advanced Photon Source, Argonne National Laboratory.[33] Both the bending magnet (BM) and the insertion device (ID) stations were used for the measurements with experiments repeated at two separate occasions. Both beamlines use Si(111) double crystal monochromators, with a water-cooled first crystal on the BM line, and a liquid-nitrogen-cooled first crystal on the ID line. X-ray harmonics were minimized on the BM line by detuning the monochromator, while a harmonic-reduction mirror was used on the ID line. The first harmonic of the undulator was used for the ID measurements.

Cr K-edge (5989 eV) fluorescence measurements at the BM line were made using 25% nitrogen and 75% helium in the incident ion chamber (I_0) which monitored the intensity of the incident beam. The transmission ion chamber (used to monitor the intensity of the beam transmitted through the sample) and reference ion chamber (used to monitor the intensity of the beam transmitted through Cr foil which was used to align and calibrate the scans) were filled with 10% Ar and 90% N_2. A Vortex 4-element Si drift detector was used to collect fluorescence data at room temperature using 15 to 30 min step scans. In the 30 min step scan, the step size for the low-resolution pre-edge region was 5 eV, whereas for the near-edge region, it was 1 eV. The region beyond about 50 eV above the edge (up to k = 16 Å^{-1}) had a step size of 0.05 Å^{-1}. In the 15 min step scan, the region above the edge (up to k = 13 Å^{-1}) had a step size of 0.1 Å^{-1}. Solid $Cr(ONO)_2$ was measured using 30 min scans, while all other samples were measured using 15 min scans. Calibration measurements on Cr foil were made before and between scans where the sample data were gathered and were stable within 0.1 eV throughout the experiment.

The Cr K edge measurements at the ID line were carried out using 10% nitrogen and 90% helium gas in the incident ion chamber and 100% nitrogen in the transmission ion chamber. To gather the Cr reference foil data, a thin scattering foil was placed in the beam before the I_0 detector to deflect a small fraction of the beam through the foil to a PIN diode detector. The fluorescence detector (Lytle detector, without an X-ray filter) in the Stern-Heald geometry[34] filled with pure argon was used for all samples except the very thin samples of solid $Cr(ONO)_2$ and $Cr(DOPO)_2$, which were examined using the 4-element Vortex Si drift detector. Approximately 15 min step scans were used with both detectors where the monochromator and the undulator were coupled. In the Lytle step scans, the step size for the low-resolution pre-edge region was 5 eV, whereas for the near-edge region, it was 0.5 eV. The region above the edge (up to k = 16 Å^{-1}) had a step size of 0.1 Å^{-1}. In the Vortex step scans, the step sizes were changed to 1 eV in the near-edge region and to 0.05 Å^{-1} in the region above the edge (up to k = 16 Å^{-1}).

Data reduction for EXAFS analysis was performed using the methods described in the UWXAFS package.[35] The alignment and the

dx.doi.org/10.1021/ic501222n | *Inorg. Chem.* 2014, 53, 10203−10216

background removal of the raw data were done using the program ATHENA[36] from the UW IFEFFIT analysis package.[37] The scans were aligned using the Cr reference spectra and merged with like scans in energy space to increase the signal-to-noise ratio. After removing the pre-edge background the spectra were normalized to have a step size of 1. The inflection points of the absorption edges were used to determine the edge energy, E_0. The EXAFS oscillations in the postedge region were isolated after subtracting the background using the AUTOBK method[38] in ATHENA. Further details of the EXAFS data analysis may be found in the Supporting Information.

X-ray Crystallography. Crystals of $Cr(ONO)_2$ were grown by slow evaporation from dichloromethane, and those of $Mo(ONO)_2$ were grown by evaporation from hexane. Crystals of $Pb(DOPO)_2 \cdot 2C_6H_6$ were grown by vapor diffusion of methanol into a benzene solution of the complex, while the group 6 $M(DOPO)_2$ crystals were grown by vapor diffusion of acetonitrile into chloroform. Crystals were placed in Paratone oil before being transferred to the cold N_2 stream of a Bruker Apex II CCD diffractometer in a nylon loop.

In all structures, data were reduced, correcting for absorption, using the program SADABS. The structures of $Mo(ONO)_2$ and $Pb(DOPO)_2 \cdot 2C_6H_6$ were solved using Patterson maps to find the metal atoms and the atoms in the first coordination sphere, with other heavy atoms found on subsequent difference Fourier maps. The structures of $W(DOPO)_2$ and those containing 3d metals were solved by direct methods, while the model derived from $W(DOPO)_2$ was used as the starting point for the isomorphous $Mo(DOPO)_2$ crystal. All nonhydrogen atoms were refined anisotropically.

In the group 6 $M(ONO)_2$ complexes, one *tert*-butyl group (centered on C28) was observed to be disordered. The disorder was modeled by constraining the thermal parameters of opposite carbons to be equal and allowing the two orientations' occupancies to refine (the major component was found to have an occupancy of 64.1(3) and 62.2(5)% in the Cr and Mo complexes, respectively). All hydrogen atoms were placed in calculated positions, except in $Cr(ONO)_2$, $Cr(DOPO)_2$, and $W(DOPO)_2$, where all hydrogen atoms except those on the *tert*-butyl groups centered on C28 in $Cr(ONO)_2$ and on C38 in $Cr(DOPO)_2$ were located on difference Fourier maps and refined isotropically. Calculations used SHELXTL (Bruker AXS),[39] with scattering factors and anomalous dispersion terms taken from the literature.[40] Further details about the structures are given in Table 1 and Supporting Information, Table S1.

Structural Analysis of Metal ONO Complexes. Structural data of ONO complexes with unambiguous metal (and hence ligand) oxidation states were compiled from the Cambridge Structural Database (accessed 11 February 2014). Compounds with *N*-protonated or *N*-alkylated ONO ligands were excluded. The data set consisted of 41 structures containing a total of 110 crystallographically distinct aryl rings (36 with oxidation state of −1, 20 with oxidation state of −1.5, 33 with oxidation state of −2, and 21 with oxidation state of −3). References and additional details for all structures used are provided in Supporting Information, Table S2. Eight chemically distinct bond lengths were tabulated for each crystallographically independent aryl ring in the data set: the C−O and C−N bond lengths and the six C−C bond lengths. The bond lengths are tabulated in the Excel spreadsheet ONO_MOSCalculator.xls available as Supporting Information.

Values were averaged for each parameter for each oxidation state of the ligand, and the resulting averages were plotted as a function of ligand oxidation state (Figure 6). Linear correlations were adequate to express the observed relationship of distance with oxidation state in all cases; unlike the situation for amidophenoxides,[41] the data for ONO complexes do not justify a nonlinear fit for the C1−C2 distance. Since all correlations are linear, the least-squares fit to determine the metrical oxidation state can be solved analytically; the solution is given in the Supporting Information and operationalized in the ONO_MOSCalculator.xls spreadsheet.

RESULTS

Preparation of Group 6 $M(ONO)_2$ and $M(DOPO)_2$ Complexes. The typical synthetic strategy for preparing homoleptic $M(ONO)_2$ complexes is the self-assembly of the ligand from 3,5-di-*tert*-butylcatechol and ammonia in the presence of an appropriate kinetically labile metal precursor under aerobic conditions. Since chromium(II) is labile but not stable to aerobic conditions, while chromium(III) is air-stable but kinetically inert, this method fails for chromium.

We have found that $Pb(ONO^Q)_2$ is a mild and efficient reagent for the replacement of halides with the ONO^Q ligand in both main group[10] and transition metal[42] halides. This preformed source of the ONO ligand allows one to finesse the problem of the kinetic inertness of Cr(III): chromium(II) chloride reacts cleanly with $Pb(ONO^Q)_2$ in THF under anaerobic conditions to provide the desired homoleptic $Cr(ONO)_2$ complex (eq 1). The molybdenum complex $Mo(ONO)_2$ may be prepared similarly from the reaction of the readily available molybdenum(II) bromo carbonyl $Mo_2Br_4(CO)_8$ with $Pb(ONO^Q)_2$ (eq 2). The tungsten analogue, previously prepared from tungsten hexachloride and $H_3[ONO^{Cat}]$,[18] can also be prepared by the reaction of $Pb(ONO^Q)_2$ with $W_2Br_2(CO)_8$. All three compounds can be purified by chromatography on silica gel. The chromium complex is indefinitely air-stable; solutions of the molybdenum and tungsten analogues degrade in the presence of air over the course of weeks, but the compounds may be handled in air for short periods of time without decomposition.

$$CrCl_2 + Pb(ONO^Q)_2 \xrightarrow[-PbCl_2]{THF} Cr(ONO)_2 \quad 52\% \qquad (1)$$

$$^1/_2\, M_2Br_4(CO)_8 + Pb(ONO^Q)_2 \xrightarrow[-PbBr_2,\ -4\,CO]{CH_2Cl_2} M(ONO)_2 \quad (2)$$

M = Mo, 61%
M = W, 41%

Ivakhnenko, Minkin, and co-workers recently reported the preparation of an analogue of $H(ONO^Q)$[43] with a bridging oxygen in place of the 6 and 6′ hydrogens, 2,4,6,8-tetra-*tert*-butyl-9-hydroxyphenoxazin-1-one ($H(DOPO^Q)$, Figure 1b).[21] We found the published synthesis of $H(DOPO^Q)$ from 2,6-dihydroxy-3,5-di-*tert*-butylaniline and 3,5-di-*tert*-butylcatechol, in refluxing benzene using catalytic toluenesulfonic acid, to be unreliable. In contrast, treatment of the same starting materials in benzene at room temperature in the air with 10 mol % triethylamine[44] reliably gives $H(DOPO^Q)$ after precipitation from methanol, albeit in modest yields (eq 3). The protonated ligand can be used to prepare $Cr(DOPO)_2$ by reaction with chromocene, releasing 2 equiv of cyclopentadiene (eq 4).

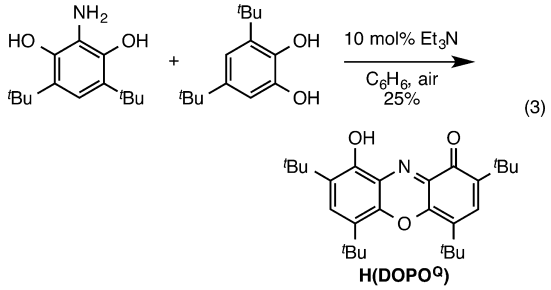

(3)

$$Cp_2Cr + 2\,H(DOPO^Q) \xrightarrow[-2\,C_5H_6]{THF} Cr(DOPO)_2 \quad 60\% \qquad (4)$$

dx.doi.org/10.1021/ic501222n | Inorg. Chem. 2014, 53, 10203−10216

To synthesize the molybdenum and tungsten dioxophenoxazine complexes, the previously unknown lead(II) complex $Pb(DOPO^{Q})_2$ was prepared as a DOPO transfer agent. Reaction of lead acetate trihydrate with $H(DOPO^{Q})$ produces $Pb(DOPO^{Q})_2$, but the reaction is slow and low-yielding because of the insolubility of both reagents in methanol. A more efficient procedure uses organic-soluble lead(II) 2-ethylhexanoate; mixing solutions of this reagent with $H(DOPO^{Q})$ in dichloromethane followed by precipitation with CH_3CN gives $Pb(DOPO^{Q})_2$ in high yield (eq 5).

$$Pb(O_2CR)_2 + H(DOPO^{Q}) \longrightarrow Pb(DOPO)_2 \quad (5)$$

R = $-CH_3$, CH_3OH, Δ, 2 d, 44%
R = $-CH(Et)CH_2CH_2CH_2CH_3$, CH_2Cl_2, RT, 80%

The coordination environment of $Pb(DOPO^{Q})_2$, like that of $Pb(ONO^{Q})_2$,[10,16] is highly distorted (Figure 3, Table 2), with

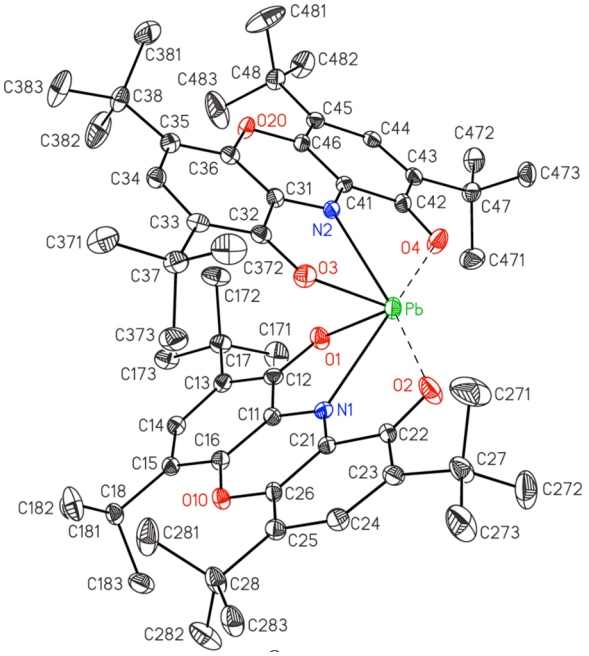

Figure 3. Thermal ellipsoid plot of $Pb(DOPO^{Q})_2 \cdot 2C_6H_6$, with hydrogen atoms and solvent molecules omitted for clarity.

two of the oxygen atoms tightly coordinated to lead (average (av) length of Pb−O = 2.319(11) Å) and two oxygens much more weakly bound (Pb−O = 2.78(3) Å av). The core N_2O_2 coordination geometry is a bent sawhorse, with O−Pb−O < 90° and N−Pb−N ≈ 120°, which is typical of lead(II) complexes of hard ligands.[45] The coordination geometry of the DOPO compound is very similar to that of the ONO analogue, with the exception of ∼0.05 Å longer Pb−O distances in the DOPO compound. In both compounds, the bonding within the ligand reflects the asymmetry of the binding of the rings, with the greater quinonoid character of the ring with the long Pb−O distance reflected in shorter C−O and C−N bonds. However, this asymmetry is more marked in the ONO complex (Δd_{C-O} = 0.073(6) Å, Δd_{C-N} = 0.058(9) Å) than it is in the DOPO complex (Δd_{C-O} = 0.051(6) Å, Δd_{C-N} = 0.028(6) Å). ^{1}H NMR spectra of $Pb(DOPO^{Q})_2$ in CD_2Cl_2 are symmetrical at all temperatures to −60 °C, suggesting that the structure is fluxional in solution.

Treatment of molybdenum(II) or tungsten(II) bromide carbonyls with $Pb(DOPO^{Q})_2$ results in immediate evolution of

Table 2. Selected Distances (Å) and Angles (deg) in $Pb(DOPO^{Q})_2 \cdot 2C_6H_6$ and $Pb(ONO^{Q})_2 \cdot 2CHCl_3$

	$Pb(DOPO^{Q})_2 \cdot 2C_6H_6$	$Pb(ONO^{Q})_2 \cdot 2CHCl_3$[a]
Pb−O1	2.327(2)	2.251(2)
Pb−O3	2.311(2)	2.258(2)
Pb−O2	2.799(2)	2.822(2)
Pb−O4	2.761(2)	2.773(2)
Pb−N1	2.583(2)	2.572(3)
Pb−N2	2.576(2)	2.592(2)
O1−C12	1.297(4)	1.304(4)
O3−C32	1.293(4)	1.301(4)
O2−C22	1.246(4)	1.229(4)
O4−C42	1.243(4)	1.231(4)
N1−C11	1.347(4)	1.374(4)
N2−C31	1.340(4)	1.367(4)
N1−C21	1.316(4)	1.307(4)
N2−C41	1.316(4)	1.318(4)
O1−Pb−O2	123.64(7)	125.22(7)
O1−Pb−O3	88.79(8)	90.09(8)
O1−Pb−O4	80.52(7)	81.81(7)
O1−Pb−N1	65.65(8)	66.90(8)
O1−Pb−N2	70.01(8)	72.83(7)
O2−Pb−O3	84.41(8)	71.33(7)
O2−Pb−O4	144.26(7)	150.51(7)
O2−Pb−N1	59.40(7)	59.12(7)
O2−Pb−N2	148.15(8)	134.19(7)
O3−Pb−O4	125.39(7)	125.49(7)
O3−Pb−N1	70.39(8)	78.26(8)
O3−Pb−N2	66.21(8)	66.64(8)
O4−Pb−N1	143.06(8)	141.41(7)
O4−Pb−N2	59.76(7)	59.43(7)
N1−Pb−N2	117.01(8)	125.63(8)

[a]Data for $Pb(ONO^{Q})_2 \cdot 2CHCl_3$ from ref 10.

CO, precipitation of $PbBr_2$, and formation of the corresponding group 6 bis(DOPO) complexes in good yield (eq 6). The $M(DOPO)_2$ complexes can be handled in air for short periods of time, but decompose over the course of several days.

$$^1/_2\, M_2Br_4(CO)_8 + Pb(DOPO^{Q})_2 \xrightarrow[-PbBr_2,\ -4\,CO]{CHCl_3} M(DOPO)_2 \quad (6)$$

M = Mo, 61%
M = W, 72%

Structure and Bonding of Molybdenum and Tungsten Complexes; Metrical Oxidation States of ONO Complexes. $Mo(ONO)_2$ adopts a distorted octahedral structure (Figure 4) and is isostructural to the previously described $W(ONO)_2$.[18] As is typical of bis(ONO) complexes,[13] the structure is roughly D_{2d}-symmetric, but its symmetry is lowered to D_2 by slight twisting of the benzene rings to minimize contacts between the 6 and 6′ hydrogens. In contrast, $W(DOPO)_2$ (Figure 5) and the isostructural $Mo(DOPO)_2$ (Supporting Information, Figure S2) adopt structures that are very close to ideal D_{2d} symmetry, with nearly coplanar ligands. The DOPO structures have markedly longer M−O distances and shorter M−N distances than the corresponding ONO complexes (Table 3), a trend that was previously observed in $Ni(DOPO)_2$ and $Zn(DOPO)_2$.[22] The elongation of the M−O bonds in DOPO complexes is likely due to the effect of the oxygen bridge "pulling back" the phenoxide oxygens. A similar shortening of the central nitrogen−metal bond has been

dx.doi.org/10.1021/ic501222n | Inorg. Chem. 2014, 53, 10203−10216

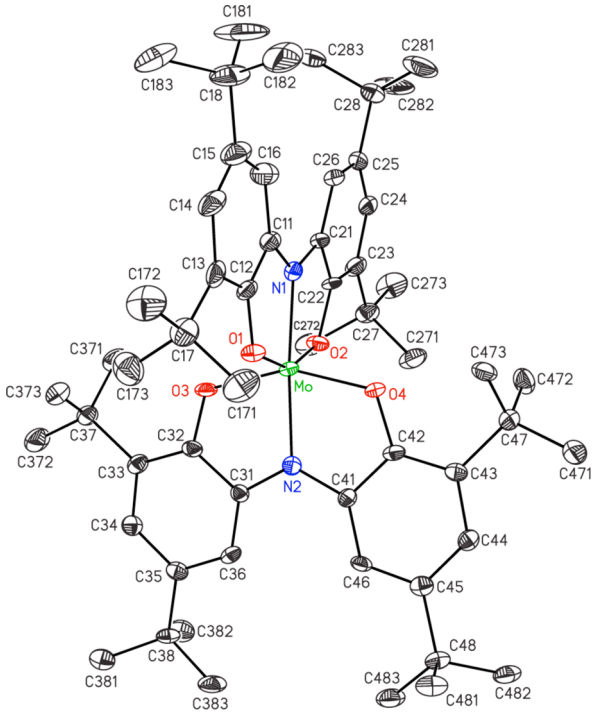

Figure 4. Thermal ellipsoid plot of $Mo(ONO)_2$. Hydrogen atoms and the minor conformation of the *tert*-butyl group centered at C28 are omitted for clarity.

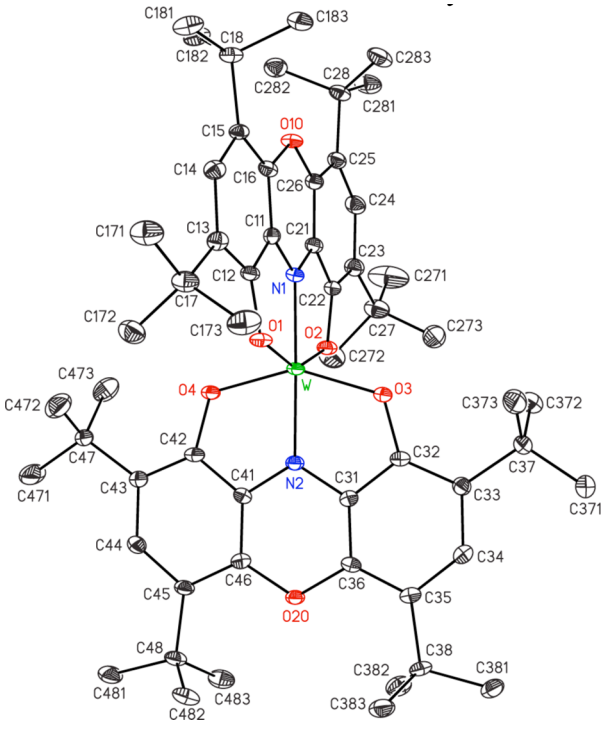

Figure 5. Thermal ellipsoid plot of $W(DOPO)_2$, with hydrogen atoms omitted for clarity.

described in metal−terpyridine complexes with consecutive five-membered chelate rings.[46]

To judge the oxidation states of complexes of redox-active ligands, chemists rely heavily on intraligand bond distances.[47] Given a sufficient database of structures with unambiguous oxidation states, one can make these qualitative correlations

Table 3. Selected Bond Distances (Å) and Metrical Oxidation States in $M(ONO)_2$ and $M(DOPO)_2$ (M = Mo, W)

	$Mo(ONO)_2$[a]	$W(ONO)_2$[a,b]	$Mo(DOPO)_2$[a]	$W(DOPO)_2$[a]
M−O	1.922(6)	1.909(4)	1.996(4)	1.976(3)
	1.959	*1.949*	*2.046*	*2.054*
M−N	2.030(6)	2.041(5)	1.975(5)	1.9757(17)
	2.075	*2.085*	*1.983*	*1.9922*
C1−N	1.407(7)	1.414(3)	1.362(9)	1.372(4)
	1.402	*1.408*	*1.362*	*1.367*
C2−O	1.348(8)	1.364(3)	1.366(6)	1.376(4)
	1.344	*1.356*	*1.351*	*1.364*
C1−C2	1.400(8)	1.401(3)	1.387(8)	1.387(4)
	1.418	*1.413*	*1.402*	*1.396*
C2−C3	1.388(9)	1.390(3)	1.393(6)	1.396(4)
	1.394	*1.389*	*1.399*	*1.396*
C3−C4	1.391(8)	1.397(3)	1.402(5)	1.408(5)
	1.395	*1.397*	*1.405*	*1.406*
C4−C5	1.388(10)	1.398(4)	1.406(5)	1.412(4)
	1.399	*1.396*	*1.409*	*1.408*
C5−C6	1.380(8)	1.390(4)	1.393(6)	1.403(5)
	1.396	*1.399*	*1.392*	*1.394*
C6−C1	1.392(9)	1.394(3)	1.391(5)	1.385(3)
	1.404	*1.402*	*1.393*	*1.389*
MOS	−2.86(13)	−3.02(9)	−2.83(23)	−3.00(22)
	−2.69(10)	*−2.88(9)*	*−2.60(18)*	*−2.80(19)*

[a]Values in Roman type are averages of chemically equivalent instances in the crystal structures. Values in italics are from DFT calculated structures (B3LYP, SDD basis set for Mo and W, 6-31G* for other atoms) for structures with hydrogen atoms replacing the *tert*-butyl groups. [b]Crystallographic data from ref 18.

quantitative and derive "metrical oxidation states" based on the intraligand bond lengths. This has the additional value that the MOS is sensitive to the degree of π bonding, since π donation depletes the ligand HOMO and gives rise to the same metrical changes as would be seen on ligand oxidation. In particular, fractional oxidation states have been seen as signatures of π-bonding effects.[41,48]

There are enough suitable ONO structures (46 structures containing 128 crystallographically distinct rings, see Supporting Information) to allow satisfactory correlations between oxidation state and bond distances (Figure 6). Since the correlations are linear, the metrical oxidation state can be determined analytically (Supporting Information, eq S1). Because the effects of ligand oxidation are delocalized over two rings, the slopes of the correlations are about half the magnitude of those observed for amidophenolates and catecholates.[41]

Metrical oxidation states for the molybdenum and tungsten bis-ONO and bis-DOPO complexes can be calculated (Table 3) and are most consistent with assigning all four complexes as M(VI) bonded to fully reduced L^{Cat}. Surprisingly, differences in metrical oxidation state between ONO and DOPO ligands are too small to detect with confidence. Density functional theory (DFT) calculations reproduce the observed trends extremely well, though calculated MOS values are uniformly about 0.2 units more positive than are experimentally observed.

Spectroscopic data are entirely consistent with the $M^{VI}(L^{Cat})_2$ formulation. All four compounds are diamagnetic and give normal ^1H and ^{13}C NMR spectra. Chemical shifts for the COM carbons in the ONO complexes (δ 167.50, 161.91 ppm) are in

dx.doi.org/10.1021/ic501222n | *Inorg. Chem.* 2014, 53, 10203−10216

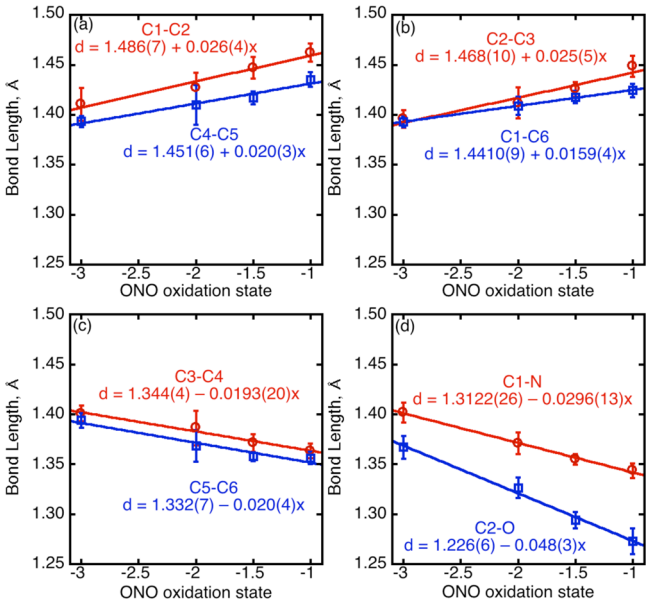

Figure 6. Correlations of bond distances with amidophenoxide oxidation state: (a) C1–C2 and C4–C5; (b) C2–C3 and C6–C1; (c) C3–C4 and C5–C6; and (d) C1–N and C2–O.

the range expected for reduced, phenoxide-like ligands.[42] The ^{1}H NMR signals for the aromatic hydrogens in the two M(DOPO^{Cat})$_2$ complexes (δ 6.62 for Mo, 6.47 for W) are about 1 ppm upfield from their shifts in any of the known diamagnetic DOPO^Q compounds (δ 7.4–7.6 ppm in $CDCl_3$).[19] This effect is tentatively ascribed to a slight paratropic shift in the DOPO^{Cat} compounds due to the weakly antiaromatic character of the reduced 16π electron phenoxazine nucleus,[49] compared to a diatropic shift in the 14π electron phenoxazinone nucleus of DOPO^Q.

Optical spectra of the four compounds show intense bands in the violet to near-UV region of the spectra (Supporting Information, Figure S7), attributed to ligand-to-metal charge transfer transitions. Absorptions at long wavelengths typical of oxidized ONO or DOPO ligands are not observed. The molybdenum compounds consistently absorb at longer wavelengths than the tungsten analogues (for ONO, λ_{max} Mo = 505 nm, W = 420 nm;[18] for DOPO, λ_{max} Mo = 463 nm, W = 412 nm). All compounds show irreversible oxidations and chemically reversible reductions in their cyclic voltammograms (Supporting Information, Figure S8). Because of the irreversibility, it is difficult to compare the oxidations of the compounds, but the differences between the DOPO and ONO ligands, and between molybdenum and tungsten, appear to be relatively small. Mo(DOPO)$_2$ is slightly more difficult to reduce than Mo(ONO)$_2$ (E° = −1.08 and −1.00 V, respectively, vs Cp_2Fe^+/Cp_2Fe) and is substantially easier to reduce than W(DOPO)$_2$ (E° = −1.54 V).

Table 4. Selected Bond Distances (Å) and Metrical Oxidation States in Cr(ONO)$_2$ and Cr(DOPO)$_2$

	Cr(ONO)$_2$[a]			Cr(DOPO)$_2$[a]		
	X-ray	DFT S = 0	DFT S = 1	X-ray	DFT S = 0	DFT S = 1
					Ligand 1[b]	
M–O	1.894(10)	*1.897*	*1.979*	2.051(9)	*1.993*	*2.127*
M–N	1.943(8)	*1.934*	*2.018*	1.9800(15)	*1.858*	*2.012*
C1–N	1.387(6)	*1.378*	*1.360*	1.322(3)	*1.342*	*1.318*
C2–O	1.324(5)	*1.314*	*1.296*	1.296(10)	*1.321*	*1.283*
C1–C2	1.418(7)	*1.432*	*1.458*	1.433(6)	*1.416*	*1.449*
C2–C3	1.422(7)	*1.408*	*1.420*	1.421(4)	*1.408*	*1.423*
C3–C4	1.384(8)	*1.386*	*1.378*	1.384(11)	*1.401*	*1.388*
C4–C5	1.409(7)	*1.411*	*1.420*	1.440(5)	*1.416*	*1.430*
C5–C6	1.381(5)	*1.387*	*1.378*	1.371(7)	*1.386*	*1.373*
C6–C1	1.403(6)	*1.412*	*1.421*	1.418(8)	*1.401*	*1.421*
MOS	−2.21(10)	*−2.08(10)*	*−1.57(11)*	−1.41(22)	*−2.08(21)*	*−1.26(21)*
					Ligand 2[b]	
			M–O	1.9915(15)	*1.993*	*2.029*
			M–N	1.8764(16)	*1.858*	*1.887*
			C1–N	1.349(2)	*1.342*	*1.344*
			C2–O	1.335(2)	*1.321*	*1.326*
			C1–C2	1.406(6)	*1.416*	*1.419*
			C2–C3	1.403(8)	*1.408*	*1.406*
			C3–C4	1.401(5)	*1.401*	*1.405*
			C4–C5	1.410(6)	*1.416*	*1.413*
			C5–C6	1.387(4)	*1.386*	*1.389*
			C6–C1	1.399(5)	*1.401*	*1.400*
			MOS	−2.33(20)	*−2.08(21)*	*−2.17(21)*

[a]Values in Roman type are averages of chemically equivalent instances in the crystal structures. Values in italics are from DFT-calculated structures (B3LYP, SDD basis set for Cr, 6-31G* for others) for the given spin states in structures with hydrogen atoms replacing the *tert*-butyl groups. [b]Ligand 1 refers to the ring containing N1 and Ligand 2 to the ring containing N2 in the crystal structure. The calculated singlet geometry of Cr(DOPO)$_2$ has D_{2d} symmetry and therefore equivalent DOPO ligands. Cr(ONO)$_2$ is observed to have approximately equivalent ligands in the solid state. Cr(ONO)$_2$ (with H in place of *tert*-butyl groups) in all spin states is calculated to have approximate D_2 symmetry and equivalent ligands. With $-CH_3$ and $-^t$Bu substituents in the 3,3′,5,5′-positions, triplet Cr(ONO)$_2$ is calculated to have both a D_2 and a C_2 local minimum, the latter with inequivalent ligands (Supporting Information, Table S3).

dx.doi.org/10.1021/ic501222n | *Inorg. Chem.* 2014, 53, 10203–10216

Solid-State Structures of $Cr(ONO)_2$ and $Cr(DOPO)_2$; Discrepancies Between Solid and Solution Properties. Crystals of $Cr(ONO)_2$ are isomorphous with those of its heavier group 6 analogues, and it adopts an analogous structure (Supporting Information, Figure S3, Table 4). The bond distances indicate significantly more oxidized (or more π-donating) ONO ligands in $Cr(ONO)_2$, MOS = −2.21(10).

In contrast, crystals of $Cr(DOPO)_2$ are not isomorphous with those of the Mo and W analogues, and the molecular structure is unique in having two DOPO ligands that are significantly different (Supporting Information, Figure S4, Table 4). One ligand (containing N2) forms short Cr−O and Cr−N bonds and is relatively reduced (MOS = −2.33(21)), with bonding quite similar to that observed in $Cr(ONO)_2$. The second ligand (containing N1) forms 0.06 Å longer Cr−O and 0.10 Å longer Cr−N bonds, and its intraligand bond distances are consistent with an apparent oxidation state that is a full unit more positive (MOS = −1.40(22)). The overall symmetry of the complex is therefore reduced from D_{2d} to C_{2v}.

The structural data, in combination with DFT calculations, provide a clear way to distinguish between different possible spin states of the chromium complexes. DFT calculations consistently indicate much shorter average metal−ligand distances in the singlet than in the triplet state (Table 4). Calculated values for both metal−ligand and intraligand bond distances for singlet $Cr(ONO)_2$ are in excellent agreement with the crystallographically observed values, while those for the triplet are not. Conversely, DFT calculations on triplet $Cr(DOPO)_2$ agree both quantitatively (metal−ligand and intraligand) and qualitatively (optimization to a C_{2v} geometry with substantially different ligand distances) with the crystallographic observations, while the computed singlet geometry is a poor match. Thus, the structural data imply that $Cr(ONO)_2$ is a singlet in the solid state, while $Cr(DOPO)_2$ is a triplet. This spin state assignment is consistent with the observed solid-state magnetic susceptibility (Figure 7). $Cr(ONO)_2$ shows essentially pure temperature-independent paramagnetism (TIP), with low susceptibility at low temperature and a linear dependence of χT with T. This is consistent with an electronic structure with no unpaired electrons, and the linear behavior argues against a significant population of excited states with unpaired electrons.[50] The magnitude of the TIP is large, but this is precedented,[51] including an example of a first-row transition metal coordinated to redox-active ligands,[52] and is not unexpected in a compound with low-lying excited states (solid $Cr(ONO)_2$ absorbs at λ > 1200 nm in its diffuse reflectance spectrum, Supporting Information, Figure S9.) In contrast, $Cr(DOPO)_2$ shows a susceptibility consistent with two unpaired electrons (μ_{eff} = 2.70 μ_B at 5 K), albeit with a small amount of TIP, giving the χT versus T plot a small positive slope.

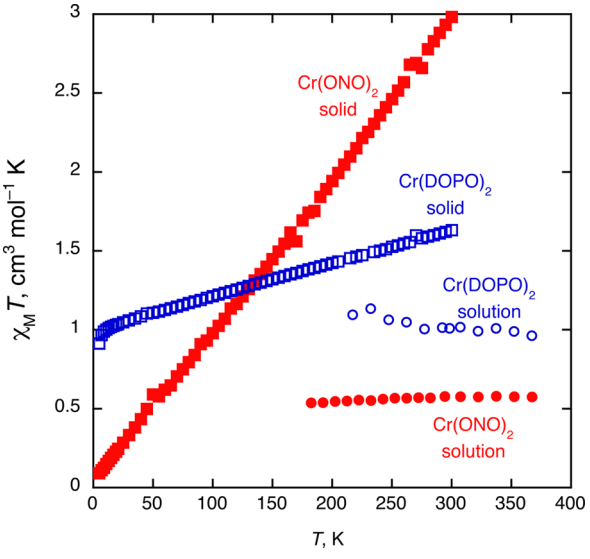

Figure 7. Magnetic susceptibilities $\chi_M T$ for solid $Cr(ONO)_2$ (red ■) and $Cr(DOPO)_2$ (blue □) and for toluene-d_8 solutions of $Cr(ONO)_2$ (red ●) and $Cr(DOPO)_2$ (blue ○).

In solution, however, $Cr(ONO)_2$ behaves quite differently than it does in the solid. Its ^1H NMR spectrum shows large downfield shifts for the two aromatic hydrogens (δ 37.55, 47.96 at room temperature in $CDCl_3$). While the large shifts might be consistent with TIP,[53] the temperature dependence of the chemical shifts (linear variation of δ with $1/T$ from 183−368 K with intercepts near the diamagnetic shifts, Figure 8) is only consistent with an S > 0 state. The linearity of these plots is strong evidence that $Cr(ONO)_2$ exhibits a single spin state in solution over this entire temperature range, in contrast to examples of spin-equilibrium in solution previously observed for $[Mn(ONO)_2]^{n+}$ (n = 0, 1)[6] or $[Co(ONO)_2]^{n+}$ (n = 0,[54] 1[55]). Consistent with this, the solution magnetic moment (Evans method) in toluene (Figure 7) is temperature-independent over this range, with μ_{eff} = 2.13 μ_B somewhat smaller than the spin-only value of 2.83 μ_B expected for an S = 1 complex. $Cr(DOPO)_2$ shows a similar paramagnetic, temperature-dependent NMR spectrum and has a solution magnetic moment of 2.86 μ_B. Both chromium compounds in solution show roughly similar, highly complex optical spectra (Supporting Information, Figure S5). Both compounds also have similar electrochemistry, each showing two reversible redox processes in CH_2Cl_2, at 0.00, −0.50 and +0.06, −0.46 V versus Fc^+/Fc for $Cr(ONO)_2$ and $Cr(DOPO)_2$, respectively (Supporting Information, Figure S6).

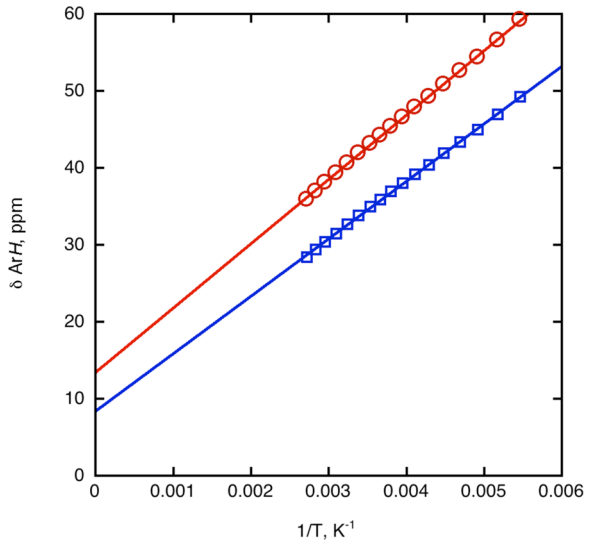

Figure 8. Chemical shifts of the two aromatic hydrogens in $Cr(ONO)_2$ (toluene-d_8).

The discrepancies between the solution and solid-state behavior of $Cr(ONO)_2$ prompted a study of the two chromium

dx.doi.org/10.1021/ic501222n | Inorg. Chem. 2014, 53, 10203−10216

compounds using Cr K-edge X-ray absorption spectroscopy (XAS). Solid-state and dissolved $Cr(ONO)_2$ show different XAS spectra in both the near-edge and EXAFS regions (Figure 9a), while spectra of solid-state and dissolved $Cr(DOPO)_2$ are

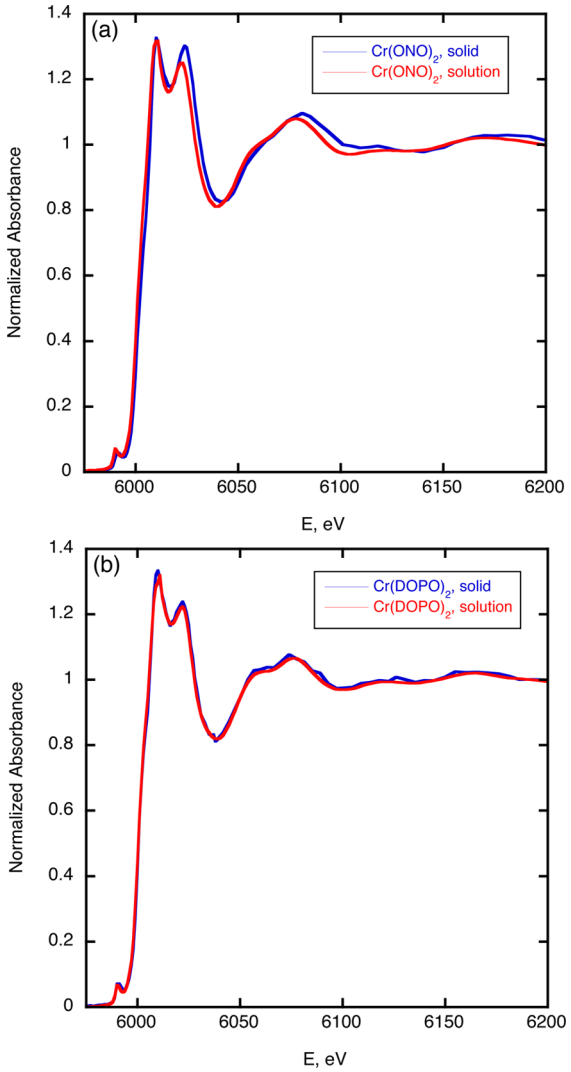

Figure 9. Cr K-edge X-ray absorption spectra of (a) $Cr(ONO)_2$ solid (blue) and as a 10 mM THF solution (red) and (b) $Cr(DOPO)_2$ solid (blue) and as a 10 mM THF solution (red).

identical (Figure 9b). In the near-edge region (Figure 10), spectra of $Cr(ONO)_2$ and $Cr(DOPO)_2$ in solution are very similar both to each other and to the chromium(III) dipicolinate complex $Na[Cr(dipic)_2]\cdot 2H_2O$, which contains a chelate that is geometrically similar to ONO and DOPO but is redox innocent. In contrast, for solid $Cr(ONO)_2$, both the weak 1s → 3d transition at ~5990 eV and the steeply rising portion of the curve associated with the 1s → 4p transition at 6000–6010 eV are shifted by approximately 1 eV to higher energy. The analogous transitions for the chromium(IV) compound CrO_2 are 1.5–2 eV higher still in energy.

Analysis of the EXAFS portion of the spectra confirms that there are detectable structural differences between $Cr(ONO)_2$ in the solid state compared to its structure in solution. In particular, the features due to scattering by the first-coordination sphere atoms are systematically shifted to longer distances in the Fourier-transformed EXAFS spectra of the

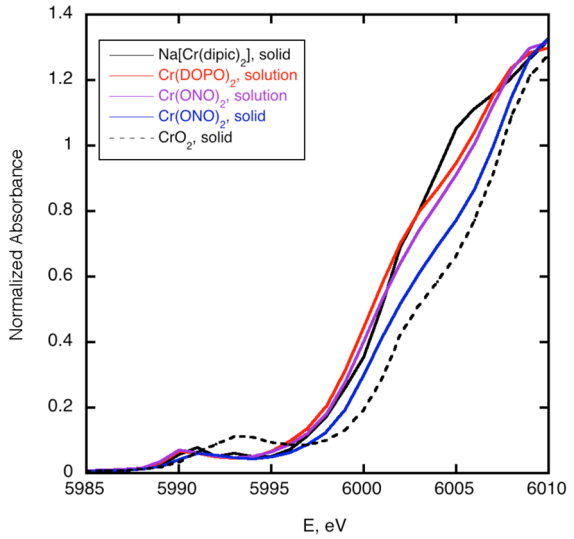

Figure 10. XANES spectra of solid $Na[Cr(dipic)_2]\cdot 2H_2O$ (solid black line), $Cr(DOPO)_2$ in THF (orange), $Cr(ONO)_2$ in THF (purple), solid $Cr(ONO)_2$ (blue), and solid CrO_2 (dashed, black).

solution-phase species compared to the solid-state compound (Figure 11). Quantitative analysis (see Supporting Information for details) indicates that the first coordination sphere is expanded, on average, by about 0.034 Å in solution compared to the solid state. However, a uniform expansion of all bond distances by this amount is not in good quantitative agreement with the data (Supporting Information, Table S6, Figure S11). The EXAFS data are consistent with either a D_2-symmetric structure with 0.022(4) Å longer Cr–O and 0.066(12) Å longer Cr–N distances than in the solid, or a C_2-symmetric structure with one ligand at very similar distances as in the solid and the other with average bond elongations of 0.064(8) Å. The structural changes are much smaller than in previously studied valence tautomers of cobalt, where changing from low-spin Co(III) to high-spin Co(II) introduces two $d\sigma^*$ electrons and leads to metal–ligand bond elongations of ~0.2 Å.[56] Computationally, the only minimum that could be located for the simplified structure with hydrogens in place of the *tert*-butyl groups is a D_2-symmetric structure (Table 4). However, calculations on the structure in which methyl groups replace the *tert*-butyls, as well as those on the full molecule, revealed both D_2 and C_2 local minima that differ in energy by less than 1 kcal/mol (Supporting Information, Table S3).

DISCUSSION

Qualitative Model of Bonding in $M(ONO)_2$ Complexes.

The redox-active orbital of the ONO ligand is principally N 2p in character, with appreciable contributions from the O 2p orbitals in phase with the nitrogen orbital, and with antibonding interactions with π-bonding orbitals of both benzene rings[20] (Figure 12a). The redox-active orbital in DOPO is similar, with the p orbital on the phenoxazine oxygen contributing in an antibonding fashion to the two benzene rings, raising the orbital in energy (Figure 12b). In both ligands, this π orbital will be the closest in energy to the metal d orbitals and will therefore dominate the π bonding with the metal. The nodal pattern of this orbital determines that as its occupancy increases, the C–O, C–N, C3–C4, and C5–C6 bonds lengthen, while the other bonds contract (Figure 6).

dx.doi.org/10.1021/ic501222n | Inorg. Chem. 2014, 53, 10203–10216

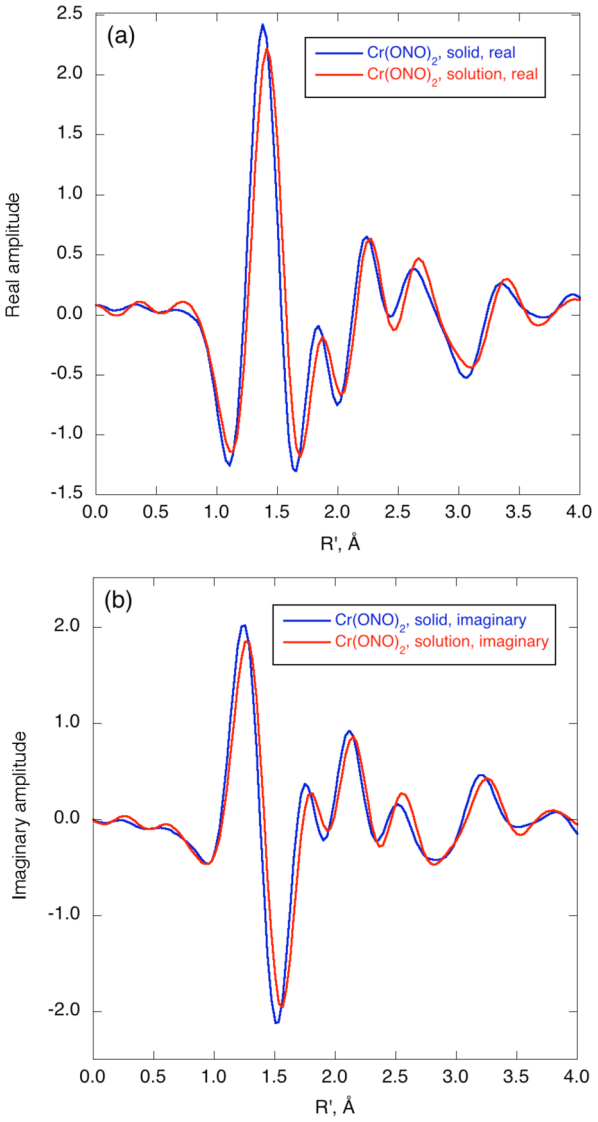

Figure 11. Fourier-transformed EXAFS spectra of $Cr(ONO)_2$ as solid (blue) and in THF solution (red). (a) Real part. (b) Imaginary part.

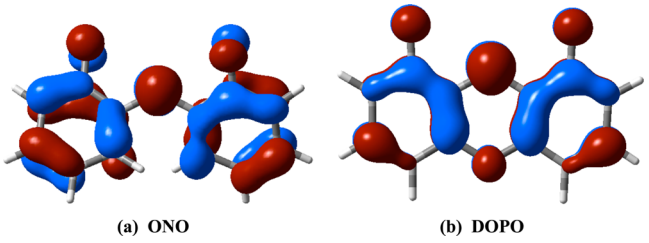

Figure 12. Kohn–Sham LUMOs (redox-active orbitals) of (a) $[ONO]^-$ (C_2-symmetric) and (b) $[DOPO]^-$ (C_{2v}-symmetric).

When interacting with the three dπ orbitals germane to an octahedral $M(ONO)_2$ complex, the two π orbitals of the ONO (or DOPO) ligands combine as shown in Figure 13. In idealized D_{2d} symmetry, the ligand π orbitals transform as an E set and interact strongly with the degenerate $\{d_{xz}, d_{yz}\}$ pair. The d_{xy} orbital, of B_1 symmetry, is nonbonding. Descent in symmetry to either D_2 or C_{2v} splits the degeneracy of the E set, but leaves d_{xy} strictly nonbonding.

The composition of the E-symmetric π and π^* orbitals depends on the relative energies of the ligand and metal

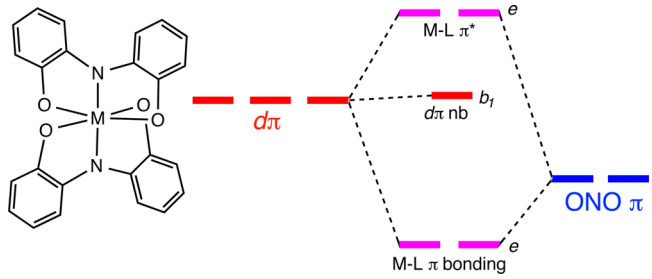

Figure 13. Qualitative π MO diagram of group 6 $M(ONO)_2$ complexes (symmetry labels from approximate D_{2d} symmetry).

orbitals. If the metal orbitals are much higher in energy than the ligand orbitals, as with early transition metals, then the π orbitals are largely ligand-centered, and the π^* orbitals are largely metal-centered. Such complexes would be appropriately viewed as containing d^0 metals, with all available electrons going to fill the ligand π orbitals. As the d orbital energies are lowered, as by moving to the right in the periodic table, the π-bonding orbitals become increasingly metal-centered.

Molybdenum and Tungsten $M(ONO)_2$ and $M(DOPO)_2$ Complexes. Molybdenum or tungsten bis(ligand) complexes have four electrons to distribute among the orbitals shown in Figure 13. All four electrons should occupy the π-bonding orbitals, which will be largely ligand-centered, in agreement with the formulation $M^{VI}(L^{Cat})_2$ and in complete agreement with all spectroscopic observations. The MOS values for all four ML_2 (M = Mo, W; L = ONO, DOPO) are close to −3, indicating that there is relatively little π donation from the ligand to the metal, which would tend to delocalize the electron density of the ligand highest-occupied molecular orbital (HOMO) onto the metal, causing intraligand bond distances to change in the same way as ligand oxidation does.[41] The molybdenum complexes show slightly more oxidized MOS values than do their tungsten analogues ($\Delta MOS \approx 0.2$). While this difference is on the edge of statistical significance, it is consistent in magnitude and direction in both ONO and DOPO complexes, and both experimentally and computationally, suggesting that it is real. This is consistent with the well-known periodic trend that the heavier transition metals are more stable (less oxidizing) in their higher oxidation states.[57] Thus, there is expected to be more charge transfer in the metal–ligand π orbital toward molybdenum than toward tungsten, resulting in lower electron density in the ligand HOMO and a more positive MOS. The same phenomenon of easier charge transfer to Mo is reflected in the relative energies of the ligand-to-metal charge transfer transitions in their optical spectra (longer wavelengths for Mo than W).

Structurally, the differences between the DOPO complexes and the ONO complexes of molybdenum and tungsten are surprisingly small, giving rise to indistinguishable MOSs (Table 3). In particular, there is no question that the DOPO ligands are well-described in these complexes as existing in their fully reduced, $[DOPO^{Cat}]^{3-}$, forms. In previous work on this ligand, all observed transition metal complexes were assigned as containing $[DOPO^{Q}]^-$ forms of the ligand,[21,22] though $Sn(DOPO)_2$ is assigned as having $[DOPO^{SQ}]^{2-}$ ligands.[58]

Electronic Structures and Valence Tautomerism in $Cr(ONO)_2$ and $Cr(DOPO)_2$. While the nature of the ligand makes surprisingly little difference in the structures of the heavier group 6 elements, it does make a difference in the structures of the chromium complexes. $Cr(DOPO)_2$ is well-

dx.doi.org/10.1021/ic501222n | Inorg. Chem. 2014, 53, 10203–10216

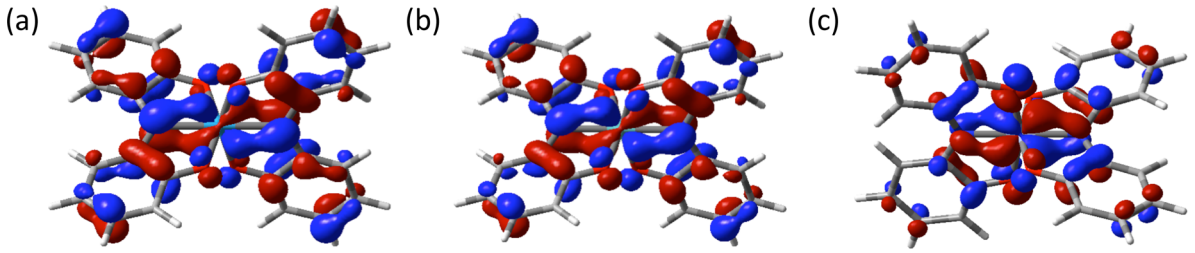

Figure 14. Kohn–Sham HOMOs of (a) $W(ONO)_2$, (b) $Mo(ONO)_2$, and (c) singlet $Cr(ONO)_2$ (B3LYP, 6-31G* [ligand]/SDD [metal]).

described as having an $S = 1$ ground state, with two rather different ligands (C_{2v} symmetry). In the qualitative molecular orbital (MO) picture, the lowest-energy triplet configuration is $(\pi)^3(\mathrm{nb})^1$, which is Jahn–Teller unstable. This explains the distortion to C_{2v} symmetry, which splits the π orbitals that are degenerate in D_{2d} by making one (ligand 2, with shorter M–L distances) more strongly bonding than the other. An equivalent formulation would be a d^3 Cr(III) ion antiferromagnetically coupled to the DOPO semiquinone ligand. This oxidation state assignment is roughly consistent with the intraligand bond distances observed in the crystal structure (sum of ligand MOS = −3.7(3)), and agrees very well with the XANES data, which show an edge energy essentially indistiguishable from that of the redox-innocent chromium(III) dipicolinate complex $[Cr(dipic)_2]^-$. DFT calculations on the triplet state also agree with a Cr(III) formulation, with Mulliken spin densities of 2.81 on Cr and of 0.05 and −0.86 on ligands 1 and 2, respectively, consistent with antiferromagnetic coupling with ligand 2. Both magnetic susceptibility measurements and Cr K-edge X-ray absorption spectroscopy indicate that the solid-state structure is retained in solution. The solution structure of $Cr(ONO)_2$, as judged by XANES, magnetic susceptibility, cyclic voltammetry, ^{1}H NMR, and UV–vis–NIR spectroscopy, appears to be similar to that of $Cr(DOPO)_2$.

The solid-state structure of $Cr(ONO)_2$, however, does not resemble that of $Cr(DOPO)_2$. Chromium–nitrogen and chromium–oxygen distances are short in $Cr(ONO)_2$, and solid-state magnetic susceptibility measurements show only temperature-independent paramagnetism, consistent with a low-spin, singlet ground state. This is supported by DFT calculations on the singlet structure, which accurately reproduce the metal–ligand and intraligand distances.

Assignment of the oxidation states in solid-state $Cr(ONO)_2$ is more challenging than the corresponding assignment of the solution state species. The metrical oxidation state of the ligands is −2.21(10), consistent with the metal center being somewhat more oxidized than the +4 state. The Cr XANES data show a chromium center significantly more oxidized than any of the Cr(III) compounds, but significantly less oxidized than the Cr(IV) standard CrO_2. While it is not in perfect agreement with the physical data, one could without gross injustice assign a Cr(IV) oxidation state to solid-state $Cr(ONO)_2$. Positing strong antiferromagnetic coupling between two unpaired spins on Cr(IV) and two on the ONO^{SQ} ligands then explains the observed singlet ground state.

The disadvantage of this assignment is that it obscures the apparent kinship between the electronic structures of $Cr(ONO)_2$ and its heavier congeners. All of the data are consistent with the same *qualitative* electronic structure of $W(ONO)_2$ and $Mo(ONO)_2$ being retained in $Cr(ONO)_2$. The differences observed are in line with the periodic trends of the transition series, where the dπ orbital energies increase down the column.[59] The corresponding redistribution of electron density in the metal–ligand π-bonding orbitals (Figure 14) results in ligand MOS values that become more positive in the order Cr ≫ Mo > W. This covalent description does not necessarily imply any integer oxidation state, and explains why different physical techniques may report different apparent oxidation states.

Studies of group 6 di-*tert*-butylimido complexes reveal analogous periodic trends, with the degree of electron density at nitrogen decreasing in the order of W > Mo ≫ Cr.[60] In the imido complexes, there is no oxidation state ambiguity; electron density is transferred from the imido to the metal through π donation. An electron-rich redox-active ligand such as ONO^{3-} or $DOPO^{3-}$, in contrast, has two possible outcomes when bonded to an oxidizing metal center such as Cr(VI). It may transfer electrons, resulting in a formal change in oxidation state; this appears to describe the situation well in the triplet compounds $Cr(DOPO)_2$ and $Cr(ONO)_2$ in solution. Or, like the imido group, it may transfer its electron density via covalent π donation to the metal. This appears to be the best description of solid, singlet $Cr(ONO)_2$. As witnessed by the stability of the two spin states under very similar conditions, both outcomes can be viable and must be considered when describing the bonding of complexes of redox-active ligands.

■ CONCLUSIONS

Reaction of divalent group 6 precursors with sources of the oxidized forms of the ligands, namely $Pb(ONO^Q)_2$, $H(DOPO^Q)$, or $Pb(DOPO^Q)_2$, serves as a general synthetic route to homoleptic redox-active ligand complexes ML_2. The molybdenum and tungsten complexes are octahedral and are well-described as M(VI) complexes of fully reduced, trianionic L^{Cat}. $Cr(DOPO)_2$ shows a novel C_{2v} structure with localized $DOPO^{SQ}$ and $DOPO^Q$ ligands coordinated to a Cr(III) center. Magnetic susceptibility measurements and X-ray absorption spectroscopy indicate that this structure is retained in solution. In contrast, analogous measurements indicate that $Cr(ONO)_2$ adopts a singlet structure with shorter metal–ligand bond lengths in the solid but a triplet structure with longer metal–ligand bond lengths in solution. The latter is similar to $Cr(DOPO)_2$, but the former defies simple oxidation state assignment. It is best described in an MO framework that emphasizes the formation of two metal–ligand π bonds and provides a unified picture for understanding the bonding in all of the group 6 complexes.

■ ASSOCIATED CONTENT

Ⓢ Supporting Information

Details on MOS analysis, electrochemistry, optical spectroscopy, EXAFS analysis, DFT calculations (PDF format), a spreadsheet implementing the MOS calculations for ONO

dx.doi.org/10.1021/ic501222n | *Inorg. Chem.* 2014, 53, 10203–10216

ligands (.xls format), and crystallographic information in CIF format. This material is available free of charge via the Internet at http://pubs.acs.org.

AUTHOR INFORMATION

Corresponding Author

*E-mail: Seth.N.Brown.114@nd.edu.

Notes

The authors declare no competing financial interest.

ACKNOWLEDGMENTS

We thank Dr. A. Oliver for assistance with the X-ray crystallography. This work was supported by the National Science Foundation (CHE-1112356). MRCAT operations are supported by the Department of Energy and the MRCAT member institutions. Use of the Advanced Photon Source, an Office of Science User Facility operated for the U.S. Department of Energy (DOE) Office of Science by Argonne National Laboratory, was supported by the U.S. DOE under Contract No. DE-AC02-06CH11357. We thank S. Chattopadhyay, T. Shibata, J. Katsoudas, and V. Zyryanov for their assistance with the XAS measurements and A. Showalter for help with the EXAFS data analysis.

REFERENCES

(1) (a) Chirik, P. J. *Inorg. Chem.* **2011**, *50*, 9737−9740. (b) Kaim, W. *Eur. J. Inorg. Chem.* **2012**, 343−348.

(2) (a) Stegmann, H. B.; Scheffler, K. *Chem. Ber.* **1970**, *103*, 1279−1285. (b) Stegmann, H. B.; Scheffler, K.; Stöcker, F. *Angew. Chem., Int. Ed.* **1970**, *9*, 456. (c) Stegmann, H. B.; Scheffler, K.; Stöcker, F. *Angew. Chem., Int. Ed.* **1971**, *10*, 499−500. (d) Uber, W.; Stegmann, H. B.; Scheffler, K.; Strähle, J. *Z. Naturforsch., B* **1977**, *32b*, 355−356.

(3) (a) Chaudhuri, P.; Hess, M.; Weyhermüller, T.; Wieghardt, K. *Angew. Chem., Int. Ed.* **1999**, *38*, 1095−1098. (b) Zarkesh, R. A.; Ziller, J. W.; Heyduk, A. F. *Angew. Chem., Int. Ed.* **2008**, *47*, 4715−4718. (c) Zarkesh, R. A.; Heyduk, A. F. *Organometallics* **2009**, *28*, 6629−6631. (d) Heyduk, A. F.; Zarkesh, R. A.; Nguyen, A. I. *Inorg. Chem.* **2011**, *50*, 9849−9863. (e) Zarkesh, R. A.; Heyduk, A. F. *Organometallics* **2011**, *30*, 4890−4898. (f) Lu, F.; Zarkesh, R. A.; Heyduk, A. F. *Eur. J. Inorg. Chem.* **2012**, 467−470.

(4) Simpson, C. L.; Boone, S. R.; Pierpont, C. G. *Inorg. Chem.* **1989**, *28*, 4379−4385.

(5) Bruni, S.; Caneschi, A.; Cariati, F.; Delfs, C.; Dei, A.; Gatteschi, D. *J. Am. Chem. Soc.* **1994**, *116*, 1388−1394.

(6) Ruiz-Molina, D.; Wurst, K.; Hendrickson, D. N.; Rovira, C.; Veciana, J. *Adv. Funct. Mater.* **2002**, *12*, 347−351.

(7) Girgis, A. Y.; Balch, A. L. *Inorg. Chem.* **1975**, *14*, 2724−2727.

(8) Camacho-Camacho, C.; Merino, G.; Martínez-Martínez, F. J.; Nöth, H.; Contreras, R. *Eur. J. Inorg. Chem.* **1999**, 1021−1027.

(9) Keller, K. A.; Connor, D. M.; Lever, J. G. U.S. Patent 2007/0117893, May 24, 2007.

(10) Shekar, S.; Brown, S. N. *Organometallics* **2013**, *32*, 556−564.

(11) Larsen, S. K.; Pierpont, C. G. *J. Am. Chem. Soc.* **1988**, *110*, 1827−1832.

(12) Speier, G.; Csihony, J.; Whalen, A. M.; Pierpont, C. G. *Inorg. Chem.* **1996**, *35*, 3519−3524.

(13) Chaudhuri, P.; Hess, M.; Hildenbrand, K.; Bill, E.; Weyhermüller, T.; Wieghardt, K. *Inorg. Chem.* **1999**, *38*, 2781−2790.

(14) Piskunov, A. V.; Trofimova, O. Y.; Ketkov, S. Y.; Fukin, G. K.; Cherkasov, V. K.; Abakumov, G. A. *Russ. Chem. Bull.* **2011**, *60*, 2522−2530.

(15) Cipressi, J.; Brown, S. N. *Chem. Commun.* **2014**, *50*, 7956−7959.

(16) McGarvey, B. R.; Ozarowski, A.; Tian, Z.; Tuck, D. G. *Can. J. Chem.* **1995**, *73*, 1213−1222.

(17) Bencini, A.; Ciofini, I.; Giannasi, E.; Daul, C. A.; Doclo, K. *Inorg. Chem.* **1998**, *37*, 3719−3725.

(18) Shaffer, D. W.; Szigethy, G.; Ziller, J. W.; Heyduk, A. F. *Inorg. Chem.* **2013**, *52*, 2110−2118.

(19) Lyubchenko, S. N.; Kogan, V. A.; Olekhnovich, L. P. *Russ. J. Coord. Chem.* **1996**, *22*, 534−539.

(20) Ren, T. *Inorg. Chim. Acta* **1995**, *229*, 195−202.

(21) Simakov, V. I.; Gorbanev, Y. Y.; Ivakhnenko, T. E.; Zaletov, V. G.; Lyssenko, K. A.; Starikova, Z. A.; Ivakhnenko, E. P.; Minkin, V. I. *Russ. Chem. Bull.* **2009**, *58*, 1361−1370.

(22) Ivakhnenko, E. P.; Starikov, A. G.; Minkin, V. I.; Lyssenko, K. A.; Antipin, M. Y.; Simakov, V. I.; Korobov, M. S.; Borodkin, G. S.; Knyazev, P. A. *Inorg. Chem.* **2011**, *50*, 7022−7032.

(23) Malkov, A. V.; Baxendale, I. R.; Dvořák, D.; Mansfield, D. J.; Kočovsky, P. *J. Org. Chem.* **1999**, *64*, 2737−2750.

(24) Cotton, F. A.; Falvello, L. R.; Meadows, J. H. *Inorg. Chem.* **1985**, *24*, 514−517.

(25) (a) Stegmann, H. B.; Scheffler, K. *Chem. Ber.* **1968**, *101*, 262−271. (b) Klein, R. F. X.; Bargas, L. M.; Horak, V. *J. Org. Chem.* **1988**, *53*, 5994−5998. (c) Bhattacharya, S.; Pierpont, C. G. *Inorg. Chem.* **1992**, *31*, 2020−2029.

(26) (a) Kahn, O. *Molecular Magnetism;* VCH: New York, 1993. (b) McElfresh, M. *Fundamentals of Magnetism and Magnetic Measurements Featuring Quantum Design's Magnetic Property Measurement System;* Quantum Design: San Diego, CA, 1994.

(27) (a) Sur, S. K. *J. Magn. Reson.* **1989**, *82*, 169−173. (b) Schubert, E. M. *J. Chem. Educ.* **1992**, *69*, 62.

(28) Ostfeld, D.; Cohen, I. A. *J. Chem. Educ.* **1972**, *49*, 829.

(29) McLinden, M. O.; Splett, J. D. *J. Res. Natl. Inst. Stand. Technol.* **2008**, *113*, 29−67.

(30) Connelly, N. G.; Geiger, W. E. *Chem. Rev.* **1996**, *96*, 877−910.

(31) Frisch, M. J.; Trucks, G. W.; Schlegel, H. B.; Scuseria, G. E.; Robb, M. A.; Cheeseman, J. R.; Scalmani, G.; Barone, V.; Mennucci, B.; Petersson, G. A.; Nakatsuji, H.; Caricato, M.; Li, X.; Hratchian, H. P.; Izmaylov, A. F.; Bloino, J.; Zheng, G.; Sonnenberg, J. L.; Hada, M.; Ehara, M.; Toyota, K.; Fukuda, R.; Hasegawa, J.; Ishida, M.; Nakajima, T.; Honda, Y.; Kitao, O.; Nakai, H.; Vreven, T.; Montgomery, J. A., Jr.; Peralta, J. E.; Ogliaro, F.; Bearpark, M.; Heyd, J. J.; Brothers, E.; Kudin, K. N.; Staroverov, V. N.; Kobayashi, R.; Normand, J.; Raghavachari, K.; Rendell, A.; Burant, J. C.; Iyengar, S. S.; Tomasi, J.; Cossi, M.; Rega, N.; Millam, J. M.; Klene, M.; Knox, J. E.; Cross, J. B.; Bakken, V.; Adamo, C.; Jaramillo, J.; Gomperts, R.; Stratmann, R. E.; Yazyev, O.; Austin, A. J.; Cammi, R.; Pomelli, C.; Ochterski, J. W.; Martin, R. L.; Morokuma, K.; Zakrzewski, V. G.; Voth, G. A.; Salvador, P.; Dannenberg, J. J.; Dapprich, S.; Daniels, A. D.; Farkas, O.; Foresman, J. B.; Ortiz, J. V.; Cioslowski, J.; Fox, D. J. *Gaussian09, Revision A.02;* Gaussian, Inc.: Wallingford, CT, 2009.

(32) Hoggard, P. E.; Schmidtke, H.-H. *Inorg. Chem.* **1973**, *12*, 1986−1990.

(33) (a) Segre, C. U.; Leyarovska, N. E.; Chapman, L. D.; Lavender, W. M.; Plag, P. W.; King, A. S.; Kropf, A. J.; Bunker, B. A.; Kemner, K. M.; Dutta, P.; Duran, R. S.; Kaduk, J. *AIP Conf. Proc.* **2000**, *521*, 419−422. (b) Kropf, A. J.; Katsoudas, J.; Chattopadhyay, S.; Shibata, T.; Lang, E. A.; Zyryanov, V. N.; Ravel, B.; McIvor, K.; Kemner, K. M.; Scheckel, K. G.; Bare, S. R.; Terry, J.; Kelly, S. D.; Bunker, B. A.; Segre, C. U. *AIP Conf. Proc.* **2010**, *1234*, 299−302.

(34) Stern, E. A.; Heald, S. M. *Handbook Sync. Rad.* **1983**, *10*, 995−1014.

(35) Stern, E. A.; Newville, M.; Ravel, B.; Yacoby, Y.; Haskel, D. *Phys. B* **1995**, *209*, 117−120.

(36) Ravel, B.; Newville, M. *J. Synchrotron Radiat.* **2005**, *12*, 537−541.

(37) Newville, M. *J. Synchrotron Radiat.* **2001**, *8*, 322−324.

(38) Newville, M.; Livins, P.; Yacoby, Y.; Rehr, J. J.; Stern, E. A. *Phys. Rev. B* **1993**, *47*, 14126−14131.

(39) Sheldrick, G. M. *Acta Crystallogr., Sect. A* **2008**, *A64*, 112−122.

(40) *International Tables for Crystallography;* Kluwer Academic Publishers: Dordrecht, The Netherlands, 1992, Vol *C*.

(41) Brown, S. N. *Inorg. Chem.* **2012**, *51*, 1251−1260.

(42) Wright, D. D.; Brown, S. N. *Inorg. Chem.* **2013**, *52*, 7831−7833.

(43) Poddel'sky, A. I.; Vavilina, N. N.; Somov, N. V.; Cherkasov, V. K.; Abakumov, G. A. *J. Organomet. Chem.* **2009**, *694*, 3462−3469.
(44) (a) Ley, K.; Lober, F. FRG Pat. 1119297, Dec. 14, 1961. (b) Maslovskaya, L. A.; Petrikevich, D. K.; Timoshchuk, V. A.; Shadyro, O. I. *Russ. J. Gen. Chem.* **1996**, *66*, 1842−1846. (c) Chaudhuri, P.; Verani, C. N.; Bill, E.; Bothe, E.; Weyhermüller, T.; Wieghardt, K. *J. Am. Chem. Soc.* **2001**, *123*, 2213−2223. (d) Shadyro, O. I.; Sorokin, V. L.; Ksendova, G. A.; Polozov, G. I.; Nikolaeva, S. N.; Pavlova, N. I.; Savinova, O. V.; Boreko, E. I. *Pharm. Chem. J.* **2003**, *37*, 399−401. (e) Mukherjee, S.; Weyhermüller, T.; Bothe, E.; Wieghardt, K.; Chaudhuri, P. *Dalton Trans.* **2004**, 3842−3853. (f) Mukherjee, C.; Weyhermüller, T.; Bothe, E.; Chaudhuri, P. *Inorg. Chem.* **2008**, *47*, 11620−11632. (g) Kopec, J. A.; Shekar, S.; Brown, S. N. *Inorg. Chem.* **2012**, *51*, 1239−1250.
(45) Davidovich, R. L.; Stavila, V.; Marinin, D. V.; Voit, E. I.; Whitmire, K. H. *Coord. Chem. Rev.* **2009**, *253*, 1316−1352.
(46) Brown, S. N. *Inorg. Chem.* **2000**, *39*, 378−381.
(47) (a) Pierpont, C. G.; Buchanan, R. M. *Coord. Chem. Rev.* **1981**, *38*, 45−87. (b) Pierpont, C. G.; Lange, C. W. *Prog. Inorg. Chem.* **1994**, *41*, 331−442. (c) de Bruin, B.; Bill, E.; Bothe, E.; Weyhermüller, T.; Wieghardt, K. *Inorg. Chem.* **2000**, *39*, 2936−2947. (d) Chun, H.; Chaudhuri, P.; Weyhermüller, T.; Wieghardt, K. *Inorg. Chem.* **2002**, *41*, 790−795. (e) Bhattacharya, S.; Gupta, P.; Basuli, F.; Pierpont, C. G. *Inorg. Chem.* **2002**, *41*, 5810−5816. (f) Schaub, T.; Radius, U. *Z. Anorg. Allg. Chem.* **2006**, *632*, 807−813. (g) Muresan, N.; Chlopek, K.; Weyhermüller, T.; Neese, F.; Wieghardt, K. *Inorg. Chem.* **2007**, *46*, 5327−5337. (h) Stanciu, C.; Jones, M. E.; Fanwick, P. E.; Abu-Omar, M. M. *J. Am. Chem. Soc.* **2007**, *129*, 12400−12401. (i) Hess, C. R.; Weyhermüller, T.; Bill, E.; Wieghardt, K. *Inorg. Chem.* **2010**, *49*, 5686−5700. (j) Bowman, A. C.; Milsmann, C.; Atienza, C. C. H.; Lobkovsky, E.; Wieghardt, K.; Chirik, P. J. *J. Am. Chem. Soc.* **2010**, *132*, 1676−1684. (k) Bowman, A. C.; Milsmann, C.; Bill, E.; Lobkovsky, E.; Weyhermüller, T.; Wieghardt, K.; Chirik, P. J. *Inorg. Chem.* **2010**, *49*, 6110−6123. (l) Das, A.; Scherer, T. M.; Mobin, S. M.; Kaim, W.; Lahiri, G. K. *Chem.—Eur. J.* **2012**, *18*, 11007−11018.
(48) Deibel, N.; Schweinfurth, D.; Hohloch, S.; Delor, M.; Sazanovich, I. V.; Towrie, M.; Weinstein, J. A.; Sarkar, B. *Inorg. Chem.* **2014**, *53*, 1021−1031.
(49) (a) Anastassiou, A. G.; Kasmai, H. S.; Saadein, M. R. *Angew. Chem., Int. Ed.* **1981**, *20*, 115−116. (b) Edwards, T. E.; Cekan, P.; Reginsson, G. W.; Shelke, S. A.; Ferré-D'Amaré, A. R.; Schiemann, O.; Sigurdsson, S. T. *Nucleic Acids Res.* **2011**, *39*, 4419−4426.
(50) Carlin, R. L. *Magnetochemistry;* Springer-Verlag: New York, 1986.
(51) (a) Johannesen, R. B.; Lindberg, A. R. *J. Am. Chem. Soc.* **1954**, *76*, 5349−5350. (b) Figgis, B. N.; Lewis, J. *Prog. Inorg. Chem.* **1965**, *6*, 37−239. (c) Chatt, J.; Leigh, G. J.; Mingos, D. M. P.; Paske, R. J. *J. Chem. Soc. A* **1968**, 2636−2641. (d) Rohmer, M.-M.; Liu, I. P.-C.; Lin, J.-C.; Chiu, M.-J.; Lee, C.-H.; Lee, G.-H.; Bénard, M.; López, X.; Peng, S.-M. *Angew. Chem., Int. Ed.* **2007**, *46*, 3533−3536.
(52) Clark, K. M.; Bendix, J.; Heyduk, A. F.; Ziller, J. W. *Inorg. Chem.* **2012**, *51*, 7457−7459.
(53) (a) Chatt, J.; Leigh, G. J.; Mingos, D. M. P. *J. Chem. Soc. A* **1969**, 1674−1680. (b) Over, D. E.; Mayer, J. M. *Polyhedron* **1993**, *12*, 2593−2602. (c) Pearson, C.; Beauchamp, A. L. *Inorg. Chim. Acta* **1995**, *237*, 13−18. (d) Brown, S. N.; Mayer, J. M. *Organometallics* **1995**, *14*, 2951−2960.
(54) (a) Caneschi, A.; Cornia, A.; Dei, A. *Inorg. Chem.* **1998**, *37*, 3419−3421. (b) Cador, O.; Chabre, F.; Dei, A.; Sangregorio, C.; Van Slageren, J.; Vaz, M. G. F. *Inorg. Chem.* **2003**, *42*, 6432−6440.
(55) Ruiz-Molina, D.; Veciana, J.; Wurst, K.; Hendrickson, D. N.; Rovira, C. *Inorg. Chem.* **2000**, *39*, 617−619.
(56) (a) Adams, D. M.; Dei, A.; Rheingold, A. L.; Hendrickson, D. N. *J. Am. Chem. Soc.* **1993**, *115*, 8221−8229. (b) Roux, C.; Adams, D. M.; Itié, J. P.; Polian, A.; Hendrickson, D. N.; Verdaguer, M. *Inorg. Chem.* **1996**, *35*, 2846−2852.
(57) Sanderson, R. T. *J. Chem. Educ.* **1988**, *65*, 112−118.
(58) Romanenko, G. V.; Ivakhnenko, E. P.; Minkin, V. I.; Starikov, A. G.; Bogomyakov, A. S.; Veber, S. L. *Inorg. Chim. Acta* **2014**, *418*, 66−72.
(59) González-Blanco, Ò; Branchadell, V.; Monteyne, K.; Ziegler, T. *Inorg. Chem.* **1998**, *37*, 1744−1748.
(60) Ciszewski, J. T.; Harrison, J. F.; Odom, A. L. *Inorg. Chem.* **2004**, *43*, 3605−3617.